



Calhoun: The NPS Institutional Archive DSpace Repository

Theses and Dissertations

1. Thesis and Dissertation Collection, all items

1994-06

Study of failure in fibrous composites subjected to bending loads

Yang, Shih-Ting

Monterey, California. Naval Postgraduate School

<http://hdl.handle.net/10945/42930>

This publication is a work of the U.S. Government as defined in Title 17, United States Code, Section 101. Copyright protection is not available for this work in the United States.

Downloaded from NPS Archive: Calhoun



<http://www.nps.edu/library>

Calhoun is the Naval Postgraduate School's public access digital repository for research materials and institutional publications created by the NPS community.

Calhoun is named for Professor of Mathematics Guy K. Calhoun, NPS's first appointed -- and published -- scholarly author.

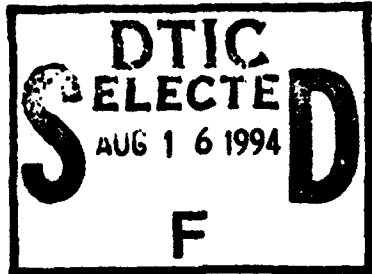
**Dudley Knox Library / Naval Postgraduate School
411 Dyer Road / 1 University Circle
Monterey, California USA 93943**

AD-A283 330



NAVAL POSTGRADUATE SCHOOL
Monterey, California

1



THESIS

DTIC QUALITY INSPECTED 2

Study of Failure in Fibrous Composites
Subjected to Bending Loads

by

Shih-Ting Yang

June, 1994

Thesis Advisor:

Young W. Kwon

Approved for public release; distribution is unlimited.

94-25696



94 8 15 081

REPORT DOCUMENTATION PAGE

Form Approved OMB No. 0704-0188

Public reporting burden for this collection of information is estimated to average 1 hour per response, including the time for reviewing instruction, searching existing data sources, gathering and maintaining the data needed, and completing and reviewing the collection of information. Send comments regarding this burden estimate or any other aspect of this collection of information, including suggestions for reducing this burden, to Washington Headquarters Services, Directorate for Information Operations and Reports, 1215 Jefferson Davis Highway, Suite 1204, Arlington, VA 22202-4302, and to the Office of Management and Budget, Paperwork Reduction Project (0704-0188) Washington DC 20503.

1. AGENCY USE ONLY		2. REPORT DATE June 1994		3. REPORT TYPE AND DATES COVERED Master's Thesis	
4. TITLE AND SUBTITLE STUDY OF FAILURE IN FIBROUS COMPOSITES SUBJECTED TO BENDING LOADS (UNCLASSIFIED)				5. FUNDING NUMBERS	
6. AUTHOR(S) Shih-Ting Yang					
7. PERFORMING ORGANIZATION NAME(S) AND ADDRESS(ES) Naval Postgraduate School Monterey CA 93943-5000				8. PERFORMING ORGANIZATION REPORT NUMBER	
9. SPONSORING/MONITORING AGENCY NAME(S) AND ADDRESS(ES)				10. SPONSORING/MONITORING AGENCY REPORT NUMBER	
11. SUPPLEMENTARY NOTES The views expressed in this thesis are those of the author and do not reflect the official policy or position of the Department of Defense or the U.S. Government.					
12a. DISTRIBUTION/AVAILABILITY STATEMENT Approved for public release; distribution is unlimited.			12b. DISTRIBUTION CODE *A		
13. ABSTRACT This study investigates the failure modes, failure strength, and failure criteria of laminated composite plate with stress concentration and subjected to bending loading. Graphite/epoxy composites are used for the present study. Lamina material properties, such as stiffness and strength, of the composite are obtained by experiments. A series of bending tests are conducted for laminated, graphite/epoxy composite plate with and without a hole to investigate their failure modes and strengths. In addition, finite element analyses are performed to compute stress distributions around holes of the composite plates subjected to bending loading. Based on the stress computation, a couple of failure criteria are examined to predict the failure strengths of composite plates with stress concentration.					
14. SUBJECT TERMS FINITE ELEMENT METHOD, DELAMINATED COMPOSITE BEAM, CONTACT-IMPACT CONDITION				15. NUMBER OF PAGES 78	
				16. PRICE CODE	
17. SECURITY CLASSIFICATION OF REPORT Unclassified	18. SECURITY CLASSIFICATION OF THIS PAGE Unclassified	19. SECURITY CLASSIFICATION OF ABSTRACT Unclassified	20. LIMITATION OF ABSTRACT UL		

NSN 7540-01-280-5500

Standard Form 298 (Rev. 2-89)

Prescribed by ANSI Std. Z39-18

Approved for public release; distribution is unlimited.

**STUDY OF FAILURE IN FIBROUS COMPOSITES
SUBJECTED TO BENDING LOADS**
by

Shih-Ting Yang

**Major, Taiwan Army
B.S, Chung Cheng Institute of Technology, August 1985**

**Submitted in partial fulfillment
of the requirements for the degree of**

MASTER OF SCIENCE IN MECHANICAL ENGINEERING

from the

**NAVAL POSTGRADUATE SCHOOL
June, 1994**

Author: _____
Shih-Ting Yang

Approved By: _____
Young W. Kwon, Thesis Advisor

Matthew D. Kelleher, Chairman
Department of Mechanical Engineering

ABSTRACT

This study investigates the failure modes, failure strengths, and failure criteria of laminated composite plates with stress concentration and subjected to bending loading. Graphite/epoxy composites are used for the present study. Lamina material properties, such as stiffness and strength, of the composite are obtained by experiments. A series of bending tests are conducted for laminated, graphite/epoxy composite plates with and without a hole to investigate their failure modes and strengths. In addition, finite element analyses are performed to compute stress distributions around holes of the composite plates subjected to bending loading. Based on the stress computation, a couple of failure criteria are examined to predict the failure strengths of composite plates with stress concentration.

Accession For	
NTIS	CRA&I
DTIC	TAB
Unannounced	
Justification	
By	
Distribution /	
Availability Codes	
Dist	Avail and / or Special
A-1	

TABLE OF CONTENTS

I.	INTRODUCTION	1
II.	LITERATURE SURVEY	3
III.	EXPERIMENT	7
	A. PLATE BENDING THEORY	7
	B. APPARATUS	18
IV.	EXPERIMENTAL RESULTS	24
	A. SPECIMENS WITHOUT A HOLE	24
	B. SPECIMENS WITH A 1/4-INCH HOLE AT THE CENTER	28
	C. CALCULATIONS FOR MATERIAL PROPERTIES	30
	D. CALCULATIONS FOR STRESS & STRESS CONCENTRATION FACTOR (SCF)	32
V.	FINITE ELEMENT ANALYSIS	43
	A. OVERVIEW	43

B. TRIANGULAR PLATE BENDING ELEMENT	
 FORMULATION	44
VI. NUMERICAL RESULTS AND DISCUSSION	51
 A. NUMERICAL RESULTS	51
 B. DISCUSSION	52
VII. CONCLUSIONS	62
APPENDIX	64
LIST OF REFERENCES	68
INITIAL DISTRIBUTION LIST	70

I. INTRODUCTION

Many of current modern technologies require materials with unusual combination of properties that cannot be met by conventional metal alloys, ceramics, and polymeric materials. This is especially true for materials that are needed for aerospace, underwater, and transportation applications. For example, aircraft engineers are increasingly searching for structural materials that are light, strong, stiff, and abrasion-, impact-, and corrosion- resistant. Rapid increase in the use of advanced composites is primarily due to their high strength-to-weight ratio and high stiffness-to-weight ratios, making them ideally suited for the high technology construction. Naval structure applications of composite materials are typically depending on this weight saving when a composite material is used to fulfill stiffness or strength requirements. The Navy has used composite materials since at least 1946 when two 28 foot personnel boats were designed using a laminated plastic. Today, composites are used widely in the fleet and include items such as submarine hatches and rudders, MK 46 torpedo propellers, minesweeper hunters, and patrol crafts [Ref. 1].

Failure of engineering materials is undesirable for several reasons; i.e., human lives that are put in jeopardy, economic losses, and the interference with the availability of products and services. Even though the causes of failure and behaviors of materials may be known, prevention of failures is difficult to guarantee. The usual causes are improper material selection and processing, inadequate design of components, and their misuse. It is the responsibility of the engineer to anticipate and plan for possible failure and, in the event that failure does occur, to assess its cause and then take appropriate preventative measures against future incidents.

The purpose of this study is to investigate the failure modes, failure strengths, and failure criteria of laminated composite plates with stress concentration and subjected to bending loading. Both experimental and numerical studies are conducted for the study. As an experimental study, four-point bending tests are undertaken to obtain lamina material properties as well as to examine failure modes and strengths of laminated composite plates with or without holes. As a numerical study, finite element analyses are performed to determine the stress distributions around the holes. A couple of failure criteria are evaluated using both the numerical and experimental studies.

II. LITERATURE SURVEY

In recent years, there have been significant studies to determine the stiffness and strength of laminated composite materials. One of the common experiments used to define the responses of composite materials is the flexure test, in which the specimen is subjected to either a central load or two quarter-point loads. In many cases, results of these tests are computed by use of formulas based upon a homogeneous material, although bi-directional (0°-90°) specimens are employed. In other words, the geometry of the stacking sequence is not taken into account.

In 1949, Hoff [Ref. 2] presented flexure formulas which, although they were based on an elementary strength of material consideration, appeared to be quite adequate to describe the bending of unidirectional or bi-directional beams. These theoretical equations, in conjunction with flexure experiments, can be utilized to calculate intrinsic material properties. Certain difficulties are still encountered in the calculations when highly anisotropic composites are tested. Pagano [Ref. 3] reviewed Hoff's equations and expressed them in a more convenient form for computational purpose.

In 1974, Hann and Tsai [Ref. 4] presented graphs to determine the laminate stiffness and strength for the $[0^\circ/+45^\circ/90^\circ]$ boron fiber/epoxy and declaimed that a set of generalized graphs for all practical laminates of a given composite can replace the current limitation of one set of graphs for each discrete laminate.

The first calculation of the effect of a circular hole on the stress concentration in a plate was published by Kirsch [Ref. 5] in 1898. He dealt with isotropic plates and computed the stress concentration factor of 3. Continuous efforts were made by many researchers to work on the stress concentration for various cases. To predict the strengths of laminated composites containing through the thickness discontinuities, two related criteria based on the normal stress distribution were developed. Whitney and Nuismer [Ref. 6] considered a circular hole of radius R in an isotropic plate of infinite extent with the origin of the x-y axes system at the center of the hole. A uniform tensile stress was applied parallel to the y-axis at infinity. As the first failure criterion, they assumed that failure occurred when the stress over a characteristic distance, d_0 , away from the discontinuity was equal to or greater than the strength of the unnotched material. They proposed the second failure criterion stating that failure

occurred when the average stress over a distance, a_0 , from the discontinuity equaled to the unnotched laminated strength. The criteria included the size effect of discontinuity. Later on, Konish and Whitney [Ref. 7] found that simply scaling the stress distribution for an isotropic plate containing a hole by a ratio of the isotropic and orthotropic stress concentration factor to get an approximate stress distribution in an orthotropic plate with a hole might lead to significant errors even close to the hole boundary, particularly if the integral of the stress distribution was used as a strength criterion in the former study. They proposed a simple polynomial which was obtained by adding sixth and eighth order terms to the isotropic solution in order to get an approximation for the normal stress distribution adjacent to a circular hole in an infinite orthotropic plate.

In 1981, Hoff and Muser calculated the stress concentration factors for circular holes in circular composite plates of cylindrical orthotropy when the outer edge of the plates were subjected to a uniform uniaxial traction. They showed that the stress concentration factor can be plotted in a diagram as a function of S_x (the compliance in radial direction) and S (two times tangential compliance plus shear compliance) if the ratio R of the plate to the diameter of the hole was prescribed. They also made a conclusion that the

stress concentration factors depended primarily on the local arrangement of the fiber at the edge of the hole [Ref. 8].

Chang and Chang [Ref. 9] presented a progressive damage model to assess damage in laminates with arbitrary ply-orientations and to predict ultimate tensile strengths of notched laminates. They developed a nonlinear finite element program for laminates containing a circular hole. They claimed a good agreement was found between the numerical prediction and the experimental data.

III. EXPERIMENT

This section explains the plate bending theory for laminated composites to obtain composite material properties from bending tests. The experimental apparatus used, the laboratory condition, and the testing procedure are also described.

A. PLATE BENDING THEORY

Because the flexural test is performed to obtain material properties of a graphite/epoxy composite, the plate bending theory for laminated composites is reviewed below.

For the classical plate bending theory, the following assumptions are made. It is assumed that the laminate thickness is small compared to its lateral dimensions. It is also assumed that there exists a perfect bonding between any two laminae. That being so, the laminae are not capable of sliding over each other and they have continuous displacements across the interface. It is made another important assumption: namely, a line originally straight and perpendicular to the laminate midplane remains so after deformation.

Finally, the so-called Kirchhoff assumption is made which states that in-plane displacements are linear functions of the thickness and interlaminar shear strains in the x-z and y-z planes are negligible. These assumptions reduce the laminate behavior to a two dimensional analysis of the laminate midplane.

The three-dimensional strain-displacement relationships are:

$$\begin{aligned}
 \epsilon_x &= \frac{\partial u}{\partial x} \\
 \epsilon_y &= \frac{\partial v}{\partial y} \\
 \epsilon_z &= \frac{\partial w}{\partial z} \\
 \epsilon_{xy} &= \frac{\partial u}{\partial y} + \frac{\partial v}{\partial x} \\
 \epsilon_{xz} &= \frac{\partial u}{\partial z} + \frac{\partial w}{\partial x} \\
 \epsilon_{yz} &= \frac{\partial v}{\partial z} + \frac{\partial w}{\partial y}
 \end{aligned} \quad \dots \dots \dots \quad (1)$$

Based on the Kirchhoff's assumption, the in-plane displacements are linear functions of the thickness coordinate z ,

where u_0 and v_0 are in-plane displacements of the midplane. From the Kirchhoff's assumption, Eq. (3) is also obtained.

It follows therefore that the vertical displacement of any point does not change in the thickness direction. Finally, the three in-plane strain components are expressed as

$$\begin{aligned}\varepsilon_x &= \frac{\partial u}{\partial x} - \frac{\partial u_0}{\partial x} - z \frac{\partial^2 w}{\partial x^2} = \varepsilon_x^0 + z k_x \\ \varepsilon_y &= \frac{\partial v}{\partial y} - \frac{\partial v_0}{\partial y} - z \frac{\partial^2 w}{\partial y^2} = \varepsilon_y^0 + z k_y \\ \varepsilon_{xy} &= \frac{\partial u}{\partial y} + \frac{\partial v}{\partial x} = \varepsilon_{xy}^0 + z k_{xy}\end{aligned} \quad \dots \quad (4)$$

where

$$\left[\begin{array}{c} 0 \\ \varepsilon_x \\ \varepsilon_y \\ 0 \\ \varepsilon_{xy} \end{array} \right] - \left[\begin{array}{c} \frac{\partial u_0}{\partial x} \\ \frac{\partial v_0}{\partial y} \\ \frac{\partial u_0}{\partial y} + \frac{\partial v_0}{\partial x} \end{array} \right]; \left[\begin{array}{c} k_x \\ k_y \\ k_{xy} \end{array} \right] - - \left[\begin{array}{c} \frac{\partial^2 w}{\partial x^2} \\ \frac{\partial^2 w}{\partial y^2} \\ 2 \frac{\partial^2 w}{\partial x \partial y} \end{array} \right]$$

Equation (4) can be expressed in the compact form as given below:

$$\begin{bmatrix} \epsilon_x \\ \epsilon_y \\ \epsilon_{xy} \end{bmatrix} = \begin{bmatrix} 0 \\ \epsilon_x \\ \epsilon_y \\ 0 \end{bmatrix} + z \begin{bmatrix} k_x \\ k_y \\ k_{xy} \end{bmatrix} \quad \dots \dots \dots (5)$$

Now, it is considered a composite made of n stacked layers or plies. Let t be the total thickness of the laminated composite plate. Then, the constitutive relationship for the k -th layer is

where $(\bar{Q})_k$ is the transformed reduced stiffness matrix. Substitution of Eq.(5) into Eq.(6) yields

Since a laminated composite is in the state of plane stress, there are three stress components. The three stress components produce the following stress resultants:

These stress resultants have the dimensions of force per unit length. These resultants give the total force per unit length acting at the midplane. Additionally, moments which are produced by the stresses with respect to the midplane are also applied at the midplane, and they are written as

$$\begin{aligned} M_x &= \int_{-l/2}^{l/2} \sigma_x z dz \\ M_y &= \int_{-l/2}^{l/2} \sigma_y z dz \\ M_{xy} &= \int_{-l/2}^{l/2} \tau_{xy} z dz \end{aligned} \quad \dots \dots \dots \quad (9)$$

From above equations, the stress resultants are written as a summation over n plies, i.e:

$$\begin{bmatrix} Nx \\ Ny \\ Nxy \end{bmatrix} = \begin{bmatrix} A_{11} & A_{12} & A_{16} \\ A_{12} & A_{22} & A_{26} \\ A_{16} & A_{26} & A_{66} \end{bmatrix} \begin{bmatrix} \epsilon_x \\ \epsilon_y \\ \epsilon_{xy} \end{bmatrix} + \begin{bmatrix} B_{11} & B_{12} & B_{16} \\ B_{12} & B_{22} & B_{26} \\ B_{16} & B_{26} & B_{66} \end{bmatrix} \begin{bmatrix} k_x \\ k_y \\ k_{xy} \end{bmatrix} \quad \dots\dots(10)$$

or

$$[N] = [A] \lceil \varepsilon^0 \rceil + [B][k] \quad \dots \dots \dots (11)$$

Similarly,

$$[M] = [B] \begin{bmatrix} \epsilon^0 \end{bmatrix} + [D][k] \quad \dots \dots \dots (12)$$

where

$$A_{ij} = \sum_{k=1}^n (\overline{Q_{ij}})_k (z_k - z_{k-1})$$

$$B_{ij} = \frac{1}{2} \left[\sum_{k=1}^n (\bar{Q}_{ij})_k (z_k^2 - z_{k-1}^2) \right] \quad \dots \dots \dots (13)$$

and

$$D_{ij} = \frac{1}{3} \left[\sum_{k=1}^n (\overline{Q_{ij}})_k (z_k^3 - z_{k-1}^3) \right]$$

Rewriting Eqs.(11) and (12) together gives

In the present study, four different laminates, $[0^\circ]_{24}$, $[90^\circ]_{24}$, $[0^\circ/90^\circ]_{12}$, and $[(+45^\circ/-45^\circ)]_8$, subjected to pure bending moments are studied. Since $[0^\circ]_{24}$ and $[90^\circ]_{24}$ laminates have similar stacking properties, they will be put into the same case to discuss:

1. Case I - $[0^\circ]_{24}$ and $[90^\circ]_{24}$ laminates:

For both $[0^\circ]_{24}$ and $[90^\circ]_{24}$ laminate composite subjected to pure bending moments, Eq.(12) becomes:

because the matrix $[B]$ will become zero for a symmetric lay-up.

That is,

Since there is no midplane stretch,

Substitution of Eq. (17) into Eq. (16) and inverse of the resultant expression gives

$$\begin{bmatrix} \epsilon_x \\ \epsilon_y \\ \epsilon_{xy} \end{bmatrix} = -z \begin{bmatrix} D_{11} & D_{12} & D_{16} \\ D_{12} & D_{22} & D_{26} \\ D_{16} & D_{26} & D_{66} \end{bmatrix}^{-1} \begin{bmatrix} M_x \\ M_y \\ M_{xy} \end{bmatrix} \quad \dots \quad (18)$$

Because D_{16} and D_{26} are equal to zero for unidirectional laminates (0° or 90°) and cross-ply laminates ($0^\circ/90^\circ$), Eq. (18) becomes:

$$\begin{bmatrix} \epsilon_x \\ \epsilon_y \\ \epsilon_{xy} \end{bmatrix} = -z \begin{bmatrix} D_{11} & D_{12} & 0 \\ D_{12} & D_{22} & 0 \\ 0 & 0 & D_{66} \end{bmatrix}^{-1} \begin{bmatrix} M_x \\ M_y \\ M_{xy} \end{bmatrix}$$

$$= -\frac{z}{\Delta} \begin{bmatrix} D_{11}^* & D_{12}^* & 0 \\ D_{12}^* & D_{22}^* & 0 \\ 0 & 0 & D_{66}^* \end{bmatrix} \begin{bmatrix} M_x \\ M_y \\ M_{xy} \end{bmatrix} \quad \dots \quad (19)$$

where:

$$\Delta = \det \begin{vmatrix} D_{11} & D_{12} & 0 \\ D_{12} & D_{22} & 0 \\ 0 & 0 & D_{66} \end{vmatrix}$$

$$D_{11}^* = D_{22} D_{66}$$

$$D_{12}^* = -D_{12} D_{66}$$

$$D_{22}^* = D_{11} D_{66} \quad \dots \quad (20)$$

$$D_{66}^* = D_{11} D_{22} - D_{12}^2$$

That is,

$$\begin{bmatrix} \epsilon_x \\ \epsilon_y \\ \epsilon_{xy} \end{bmatrix} = -\frac{z}{D_{11} D_{22} D_{66}} \begin{bmatrix} D_{22} D_{66} & -D_{12} D_{66} & 0 \\ -D_{12} D_{66} & D_{11} D_{66} & 0 \\ 0 & 0 & D_{11} D_{22} - D_{12}^2 \end{bmatrix} \begin{bmatrix} M_x \\ M_y \\ M_{xy} \end{bmatrix} \quad \dots \quad (21)$$

If subjected to a uniaxial pure bending moment: $M_x = M_0$; $M_y = M_{xy} = 0$, the strains are expressed as functions of the layer's thickness, material properties, and the bending moment. In other words,

For the four-point bending test as shown in Fig. 1,

$$M_0 = \frac{pa}{2w}$$

where :

p= load (lb)

a= length of moment arm (in)

w= plate width.

Rewriting Eq.(22) for D_{11} gives

$$D_{11} = \frac{z}{\epsilon_x} M_0 = \frac{zPa}{2\epsilon_x w} \quad \dots \dots \dots (23)$$

For $[0^\circ]_{24}$ and $[90^\circ]_{24}$ laminates, $D_{11}=2*h^3*Q_{11}/3$, $D_{12}=2*h^3*Q_{12}/3$, and $D_{22}=2*h^3*Q_{22}/3$ where h is a half of the total plate thickness. As a result:

$$Q_{11} = -\frac{3zpa}{4h^3 exw} = -\frac{3az}{4h^3 w} \left(\frac{p}{ex}\right) \quad \dots \dots \dots (24)$$

Since $\sigma_y = \tau_{xy} = 0$, Eq. (6) yields

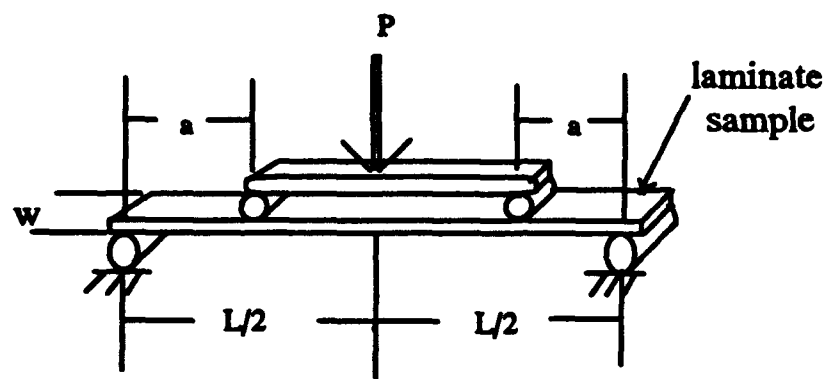


Figure 1. 4-point bending test

2. Case II - $[0^\circ/90^\circ]_{12}$ cross-ply laminate :

The derivation is similar to that for $[0^\circ]$ and $[90^\circ]$ laminates. However, since $[0^\circ/90^\circ]_{12}$ is not symmetric, the matrix $[B]$ will not reduce to zero and the situation becomes more complicated.

The stacking sequence and the thickness of each corresponding ply are shown in Fig. 2. From Equation (13), the $[A]$, $[B]$, and $[D]$ matrices for $[0^\circ/90^\circ]_{12}$ are obtained as when each layer has the same thickness.

$$\begin{aligned}
 A_{11} &= h^*[(Q_{11}) + (Q_{22})], & A_{22} &= A_{11} \\
 A_{12} &= 2h^*(Q_{12}), & A_{16} &= A_{26} = 0 \\
 A_{66} &= 2h^*(Q_{66}), \\
 B_{11} &= h^2*[(Q_{11}) + 4*(Q_{22})]/96, & B_{22} &= h^2*[4*(Q_{11}) + (Q_{22})]/96 \\
 B_{12} &= 5h^2*(Q_{12})/96, & B_{16} &= B_{26} = 0 & \dots \dots \dots (26) \\
 B_{66} &= 5h^2*(Q_{66})/96, \\
 D_{11} &= h^3*[(Q_{11}) + (Q_{22})]/3, & D_{22} &= D_{11} \\
 D_{12} &= 2h^3*(Q_{12})/3, & D_{16} &= D_{26} = 0 \\
 D_{66} &= 2h^3*(Q_{66})/3.
 \end{aligned}$$

3. Case III- $[+45^\circ/-45^\circ]$ laminates :

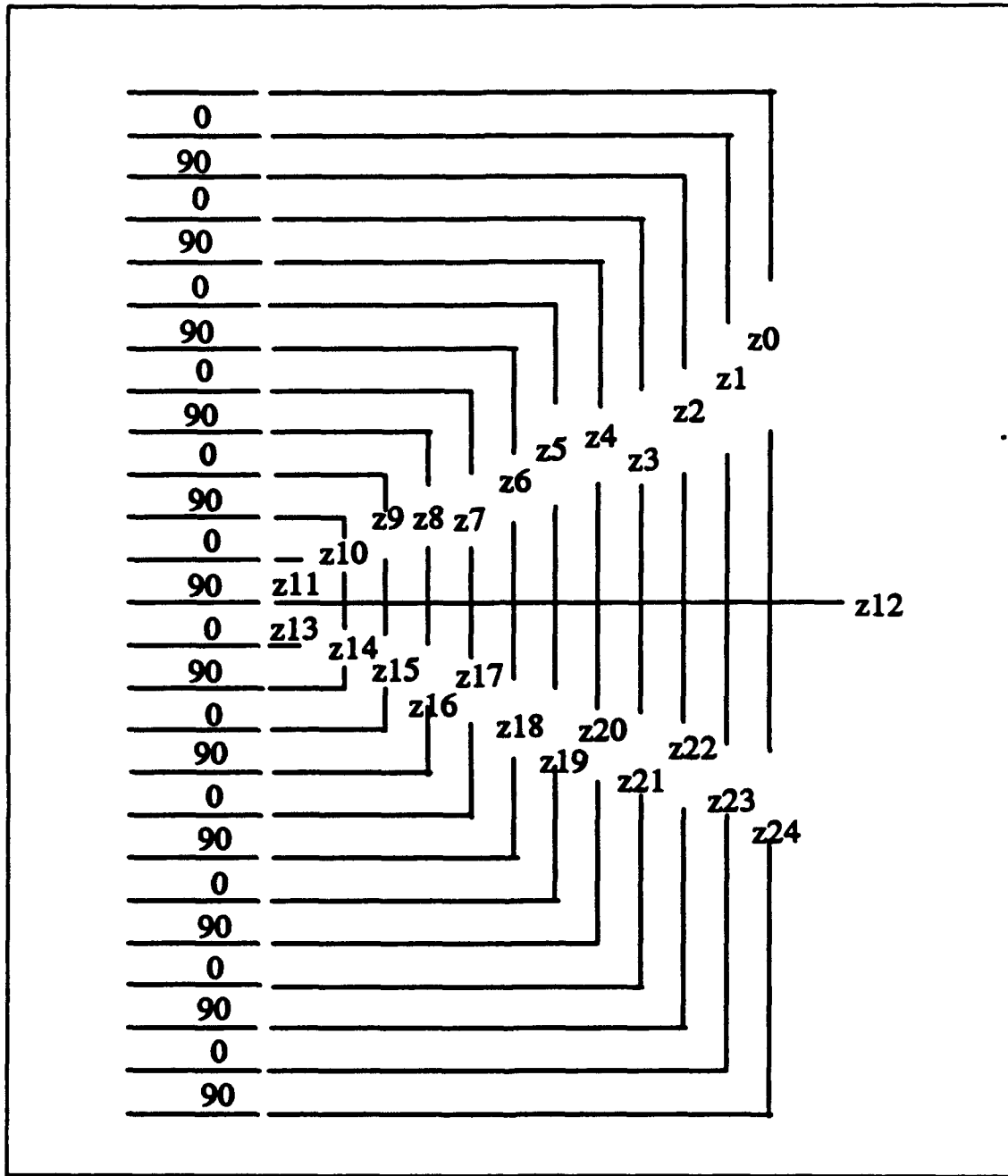


Figure 2. The stacking sequences and corresponding layer thickness of [0/90] laminate

For the $[(+45^\circ/-45^\circ)_6]$, laminated composite plate, the derivation procedure is also more complicated than the $[0^\circ]$ and $[90^\circ]$ laminates. Due to symmetry, matrix $[B]$ becomes null and the detail of matrix $[D]$ is provided below:

$$\begin{bmatrix} \epsilon_x \\ \epsilon_y \\ \epsilon_{xy} \end{bmatrix} = -\frac{z}{\Delta} \begin{bmatrix} D_{11}^* & D_{12}^* & D_{16}^* \\ D_{12}^* & D_{22}^* & D_{26}^* \\ D_{16}^* & D_{26}^* & D_{66}^* \end{bmatrix} \begin{bmatrix} M_x \\ M_y \\ M_{xy} \end{bmatrix} \quad \dots \quad (27)$$

where :

$$D_{11}^* = D_{22} D_{66} - D_{26}^2, \quad D_{12}^* = -D_{12} D_{66} + D_{16} D_{26},$$

$$D_{16}^* = D_{12} D_{26} - D_{16} D_{22}, \quad D_{22}^* = D_{11} D_{66} - D_{16}^2,$$

$$D_{26}^* = -D_{11} D_{26} + D_{12} D_{16}, \quad D_{66}^* = D_{11} D_{22} - D_{12}^2.$$

and

$$D_{11} = h^3 * [(Q_{11}) + (Q_{22}) + 2 * (Q_{12}) + 4 * (Q_{66})] / 6,$$

$$D_{22} = D_{11},$$

$$D_{12} = h^3 * [(Q_{11}) + (Q_{22}) + 2 * (Q_{12}) - 4 * (Q_{66})] / 6, \quad \dots \quad (28)$$

$$D_{16} = D_{26} = h^3 * [(Q_{11}) - (Q_{22})] / 48,$$

$$D_{66} = h^3 * [(Q_{11}) + (Q_{22}) - 2 * (Q_{12})] / 6.$$

In this thesis, Eq. (24) and the basic equations of material properties are used to compute the elastic modulii E_{11} , E_{22} ,etc. The details to calculate these elastic modulii are given in the later chapter.

B. APPARATUS

All the bending tests were conducted in a laboratory whose ambient temperature is $22.5+2.0^{\circ}\text{C}$ with an average relative humidity equal to 41+5%. The MTS 810 Material Test System was used to conduct all the bending tests.

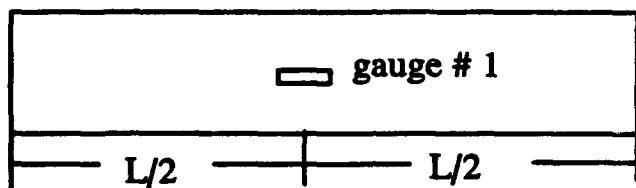
The materials used during the experimental testing were graphite fiber/epoxy composites with $[0^{\circ}]_{24}$, $[90^{\circ}]_{24}$, $[0^{\circ}/90^{\circ}]_{12}$, and $[(+45^{\circ}/-45^{\circ})_6]_s$ laminates. The experimental samples were cut from different orientation laminate plates with nominal dimensions as 12" by 12" square and 0.15" thick into small plates with length of 12" and width of 1". Some samples were drilled a quarter inch hole at the center. A fixture was designed to hold the composite samples in a simply supported configuration. Each sample was positioned on the top of the supporters. A four-point bending test was performed as shown in Fig 1.

Several strain gauges (1/4 inch CEA-13-250UN-350, with gauge factor 2.120 + 0.5%) were mounted on both sides of the samples. One strain gauge was placed at the center of each side of $[0^{\circ}]$, $[0^{\circ}/90^{\circ}]_s$, and $[+45^{\circ}/-45^{\circ}]_s$ laminae (without hole) for the purpose of obtaining the properties of laminated composite. A $[90^{\circ}]$ laminate sample (without hole) was mounted

with two strain gauges on each side, one in the longitudinal direction, and the other in the transverse direction.

Additional strain gauges were mounted on each sample with a 1/4" hole at the center to measure the strain response of the sample under load more accurately. Figures 3 to 6 show the locations of the strain gauges on each sample. Tests of these samples were conducted with the MTS material testing machine at a crosshead speed of 0.12 in/min (or 0.305 mm/min). The MTS machine provided readings and a force-displacement print-out on the x-y plotter (HP 7054A x-y Recorder) for the applied force and the measurement of the deflection of the sample. Strain gauge outputs were connected to a Measurements Group SB-10 Switch & Balance Unit, and readouts, in microstrain, provided by Measurement Group P-3500 Strain Indicator. The results were read and recorded manually upto the fracture of the sample.

on the tension side:



on the compression side:

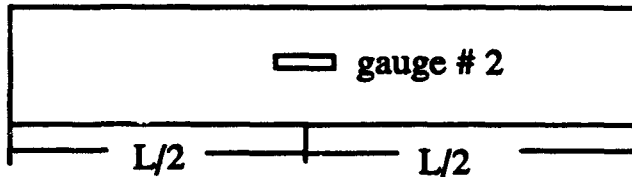
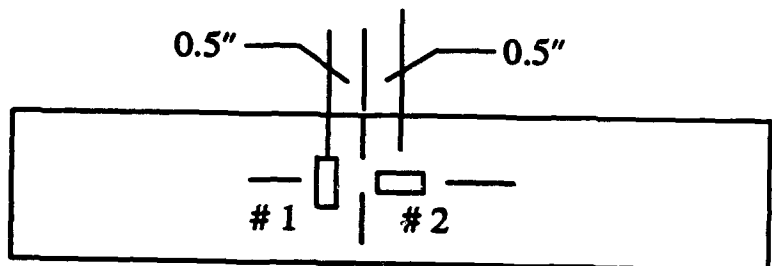


Figure 3. Strain gauge positions for [0], [0/90], and
[+45/-45] laminae without a hole

on the compression side:



on the tension side:

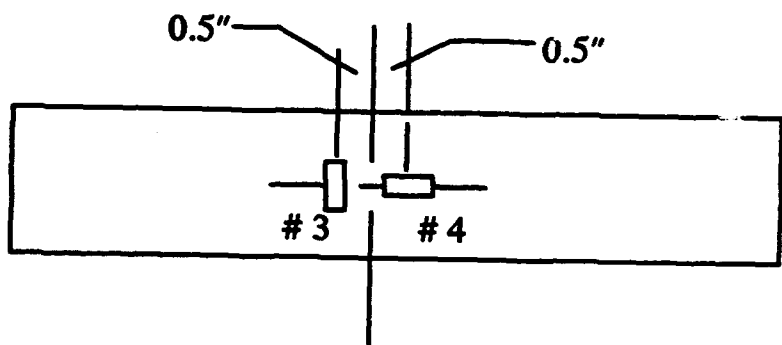


Figure 4. Strain gauge locations for [90] laminate without a hole

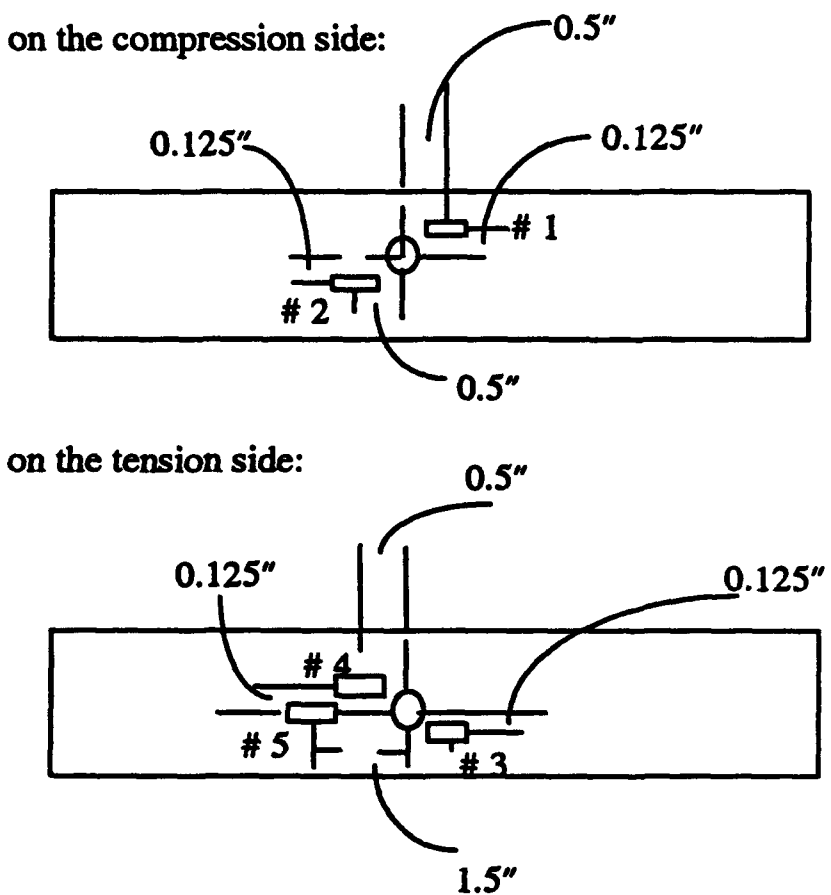
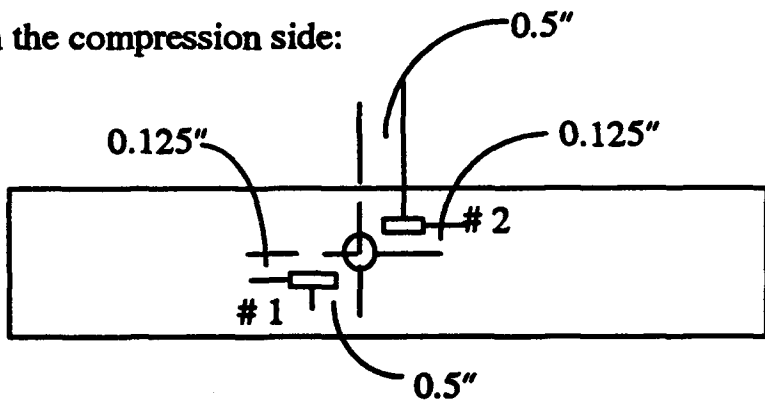


Figure 5. Strain gauge locations for [0] and [0/90] laminates with a 1/4" hole at the center

on the compression side:



on the tension side:

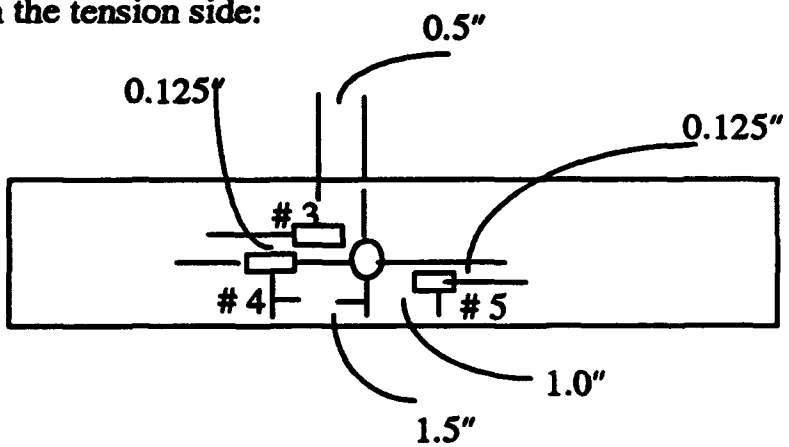


Figure 6. Strain gauge locations for [+45/-45] laminate with a 1/4" hole at the center

IV. EXPERIMENTAL RESULTS

This section presents the results as obtained from the experiments. While some description of the experimental and calculated results is provided here, a more detailed explanation and physical interpretation of the results will be given in the later chapter. In order to ensure consistency in recording loading responses, samples were placed as uniformly as possible with strain gauges in the same positions. The same crosshead speed and the same procedures were also employed for each separate test. The results are presented graphically and in a tabular form.

A. SPECIMENS WITHOUT A HOLE

The four different laminated composite samples without a hole were tested to provide a basis to compute the material properties and to compare with samples with a hole. Tables 1 to 5 show the loads and strains recorded from each experiment for the samples. The load vs. strain relationship is plotted in Figures 7 to 14.

Table 1. results for a [0] laminate without a hole

load (lb)	gauge # 1**	gauge # 2
55.5	395	-399
104	736	-745
150	1,015	-1,057
256	1,760	-1,795
298	2,035	-2,080
354	2,396	-2,456
402.5	2,712	-2,786
434	2,916	-3,001
497	3,319	-3,419
525.5	3,506	-3,617
596.5	3,950	-4,089
627	4,138	-4,289
694	4,561	-4,742
717	4,701	-4,892
780	5,082	-5,303
811.5	5,271	-5,509
887	5,729	-6,009
933	5,998	-6,305
986	6,315	-6,654
1,040	6,650	-7,007
1,070	6,836	-7,193
1,100	6,995	-7,366
1,130	7,177	-7,565
1,166	7,385	-7,779
1,200	7,558	-7,864
*		

*: failure occurred at approximate 1210 lbs.

**: see figure 3 for the strain gauge locations.

Table 2. results for a [90] laminate without a hole

load(lb)	gauge # 1**	gauge # 2	gauge # 3	gauge # 4
10	22	-941	-18	996
20	55	-2,264	-46	2,438
25	70	-2,924	-62	3,160
*				

*: failure occurred at approximate 28 lbs.

**:see figure 4 for the strain gauge locations.

Table 3. results for $[(0/90)]_{12}$ laminate without a hole

load (lb)	gauge # 1**	gauge # 2
29	-798	755
59	-1,644	1,540
90	-2,518	2,344
119.5	-3,332	3,078
149	-4,158	3,835
180	-5,015	4,601
208	-5,822	5,317
240	-6,750	6,126
267	-7,666	6,914
297	-8,652	7,749
326	-9,756	8,660
361	-11,334	9,944
391	-12,962	11,255
*		

*: failure occurred at approximate 401 lbs.

**: see figure 3 for the strain gauge locations.

Table 4. results for [+45/-45]-(1) laminate without a hole

load (lb)	gauge # 1**	gauge # 2
30	1,767	-1,803
60	4,678	-4,871
90	8,654	-9,388
107	13,759	-16,064
*		

*: no breakage occurred. quit recording due to a very large deflection.

**: see figure 3 for the strain gauge locations.

Table 5. results for [+45/-45]-(2) laminate without a hole

load (lb)	gauge # 1**	gauge # 2
4.5	339	0
29.5	1,544	-1,272
61	3,099	-2,969
90	4,576	-4,633
122	6,425	-6,805
150	8,057	-8,799
180	9,767	-10,980
210	11,795	-13,708
240	14,783	-18,065
*		

*: no breakage occurred. quit recording due to a very large deflection.

**: see figure 3 for the strain gauge locations.

B. SAMPLES WITH A 1/4-INCH HOLE AT THE CENTER

Similarly, three different laminated composite samples, $[0^\circ]$, $[(0^\circ/90^\circ)]_{12}$, and $[(+45^\circ/-45^\circ)]_{12}$ with a quarter inch hole at the center of the plate were tested. Five strain gauges were mounted with three on the tension side and two on the compression side for each sample. The three gauges on the tension side were placed with two at a distance of 0.5 in. away from the center and another one at 1.25 in. The locations of strain gauges are shown in Figures 5 and 6. The results for each sample were recorded in order to compare them with the data obtained from the previous section (section A) .

Table 6. results for a $[(+45^\circ/-45^\circ)]_{12}$ laminate with a 1/4-inch hole at the center

load (lb)	gauge # 1**	gauge # 2	gauge # 3	gauge # 4	gauge # 5
0	0	0	172	0	0
29.5	-2,910	-2,834	2,997	2,683	2,999
49.5	-5,151	-5,022	5,210	4,711	5,369
69.5	-7,834	-7,686	7,908	7,066	8,180
84.5	-10,783	-10,670	10,857	9,465	11,247
90	-12,282	-12,151	12,320	10,619	12,748
*					

*: no breakage occurred. quit recording due to a very large deflection.

**: see figure 6 for the strain gauge locations.

Table 7. results for a [0] laminate with a 1/4-inch hole at the center

load (lb)	gauge # 1**	gauge # 2	gauge # 3	gauge # 4	gauge # 5
0	0	0	167	0	0
30	-405	-428	578	444	425
49.5	-703	-736	868	753	720
72	-1,049	-1,099	1,210	1,116	1,068
91	-1,341	-1,403	1,496	1,418	1,358
112	-1,656	-1,726	1,800	1,737	1,666
133	-1,996	-2,070	2,127	2,075	1,989
152	-2,277	-2,352	2,398	2,353	2,254
171	-2,579	-2,649	2,688	2,648	2,532
190.5	-2,882	-2,949	2,977	2,943	2,813
210.5	-3,190	-3,252	3,270	3,240	3,095
230	-3,509	-3,575	3,542	3,568	3,366
250	-3,822	-4,133	3,838	4,164	3,574
270	-4,193	-4,530	4,187	4,600	3,827
290	-4,520	-4,878	4,480	4,954	4,057
310	-4,853	-5,227	4,775	5,320	*4173
320	-5,412	-5,420	5,551	5,500	*2655

*: gauge # 5 indicates failure between 310 and 320 lbs.

**: see figure 5 for the strain gauge locations.

Table 8. results for a [0/90] laminate with a 1/4-inch hole at the center

load (lb)	gauge # 1**	gauge # 2	gauge # 3	gauge # 4	gauge # 5
20.5	-552	-538	527	542	496
41	-1,110	-1,087	1,044	1,072	979
60	-1,627	-1,594	1,519	1,557	1,418
80.5	-2,184	-2,133	2,026	2,072	1,882
100.5	-2,741	-2,670	2,533	2,585	2,339
131	-3,567	-3,462	3,286	3,342	3,014
160.5	-4,363	-4,239	4,006	4,075	3,679
190	-5,165	-5,038	4,734	4,826	4,360
220	-5,998	-5,843	5,486	5,563	5,047
*					

*: failure occurred at approximate 228 lbs.

**: see figure 5 for the strain gauge locations.

C. CALCULATIONS FOR MATERIAL PROPERTIES

1. Poisson's ratio ν_{21} :

By definition, ν_{ij} is the Poisson's ratio for the transverse strain in the j -direction when stressed in the i -direction, which means

for a stress applied in the 2-direction. Applying the result of the [90°] laminate experiment to Equation(29), the average value of v_{21} is found to be 0.02225.

2. Elastic modulii E_{11} and E_{22} , & Poisson's ratio v_{12} :

Here, in order to obtain the material properties, E_{11} and E_{22} , a regression analysis using a FORTRAN program was performed to linearize the ratios of load vs. strain for [0°] and [90°] laminates. As a result,

$$(p/\epsilon_x)_{00} = \pm 154.95 \times 10^3 \quad \text{and} \quad (p/\epsilon_x)_{900} = \pm 7.245 \times 10^3$$

Since

$$\begin{aligned} Q_{11} &= \frac{E_{11}}{1-v_{12}v_{21}} \\ Q_{22} &= \frac{E_{22}}{1-v_{12}v_{21}} \\ Q_{12} &= \frac{v_{12}E_{22}}{1-v_{12}v_{21}} \end{aligned} \quad \dots \dots \dots \quad (30)$$

plugging Eq. (24) and Eq. (30) into Eq. (29) results in the following relationship:

$$\frac{E_{11}E_{22}}{E_{22}-E_{11}v_{21}^2} = \pm \left(\frac{3a}{4wh^2} \right) (p/\epsilon_x)_{00} \quad \dots \dots \dots \quad (31)$$

$$\frac{E_{22}^2}{E_{22}-E_{11}v_{21}^2} = \pm \left(\frac{3a}{4wh^2} \right) (p/\epsilon_x)_{900} \quad \dots \dots \dots \quad (32)$$

After calculations, results for these two elastic modulii are:

$$E_{11} = 6.273 \times 10^6 \text{ psi} ; E_{22} = 0.3649 \times 10^6 \text{ psi}$$

From

$$v_{12} = \frac{E_{11}}{E_{22}} v_{21}$$

we also get

$$v_{12} = 0.3825.$$

3. Shear modulus G_{12} :

A Matlab program was written in order to compute the material property, G_{12} . The experimental result of load vs. strain ratio of the $[(+45^\circ/-45^\circ)_6s]$ laminate was compared with the load vs. strain ratio calculated from the program using a guessed value of G_{12} . The Incremental Search method was employed to determine the correct guess value for G_{12} iteratively. The shear modulus G_{12} obtained from this way was $1.045 \times 10^6 \text{ psi}$.

D. CALCULATIONS FOR STRESS & STRESS CONCENTRATION FACTOR (SCF)

The failure load for each sample is shown in Table 9. Here, stresses are calculated at $z = +h$ or $-h$ (at the top or bottom of the sample) for each

sample. From Eq. (25), the failure stress for $[0^\circ]_{24}$, $[90^\circ]_{24}$, and $[(+45^\circ/-45^\circ)_6]$ laminae are

$$\sigma_{0/w_0} = 1.840 \times 10^5 \text{ psi/ per unit length,}$$

$$\sigma_{0/w} = 1.26 \times 10^5 \text{ psi/ per unit length,}$$

$$\sigma_{90/w_0} = 5.08 \times 10^3 \text{ psi/ per unit length,}$$

$$\sigma_{45/w_0} = 61.86 \times 10^3 \text{ psi/ per unit length,}$$

$$\sigma_{45/w} = 29.67 \times 10^3 \text{ psi/ per unit length.}$$

where subscripts wo and w indicate "without a hole" and "with a hole", respectively.

Table 9. dimensions and failure loads of samples

laminate	length	moment arm	failure (lb)
$[0]_{w_0}$	5"	1.5"	1,210
$[0]_w$	10"	3"	310
$[90]_{w_0}$	8"	2"	28
$[0/90]_{w_0}$	10"	3"	401
$[0/90]_w$	10"	3"	228
$[+45/-45]_{w_0}$	10"	3"	*240
$[+45/-45]_w$	10"	3"	*90

*: failure due to a very large deflection.

For $[0^\circ/90^\circ]_{12}$, the matrices [A], [B], and [D] were calculated from Eq.(26).

Plugging these data into Eq.(14) and Eq.(7), the failure stress for the $[0^\circ/90^\circ]_{12}$ laminate are

$$\sigma_{0/90-top/w0} = 213.86 \times 10^3 \text{ psi/ per unit length,}$$

$$\sigma_{0/90-bottom/w0} = 12.53 \times 10^3 \text{ psi/ per unit length,}$$

$$\sigma_{0/90-top/w} = 162.13 \times 10^3 \text{ psi/ per unit length,}$$

$$\sigma_{0/90-bottom/w} = 9.49 \times 10^3 \text{ psi/ per unit length.}$$

Based on these data, the experimental stress concentration factors (SCF) for laminated composites are 1.46 for the unidirectional plate and 1.32 for the cross-ply plate if the failure occurs due to the largest stress at an edge of the hole.

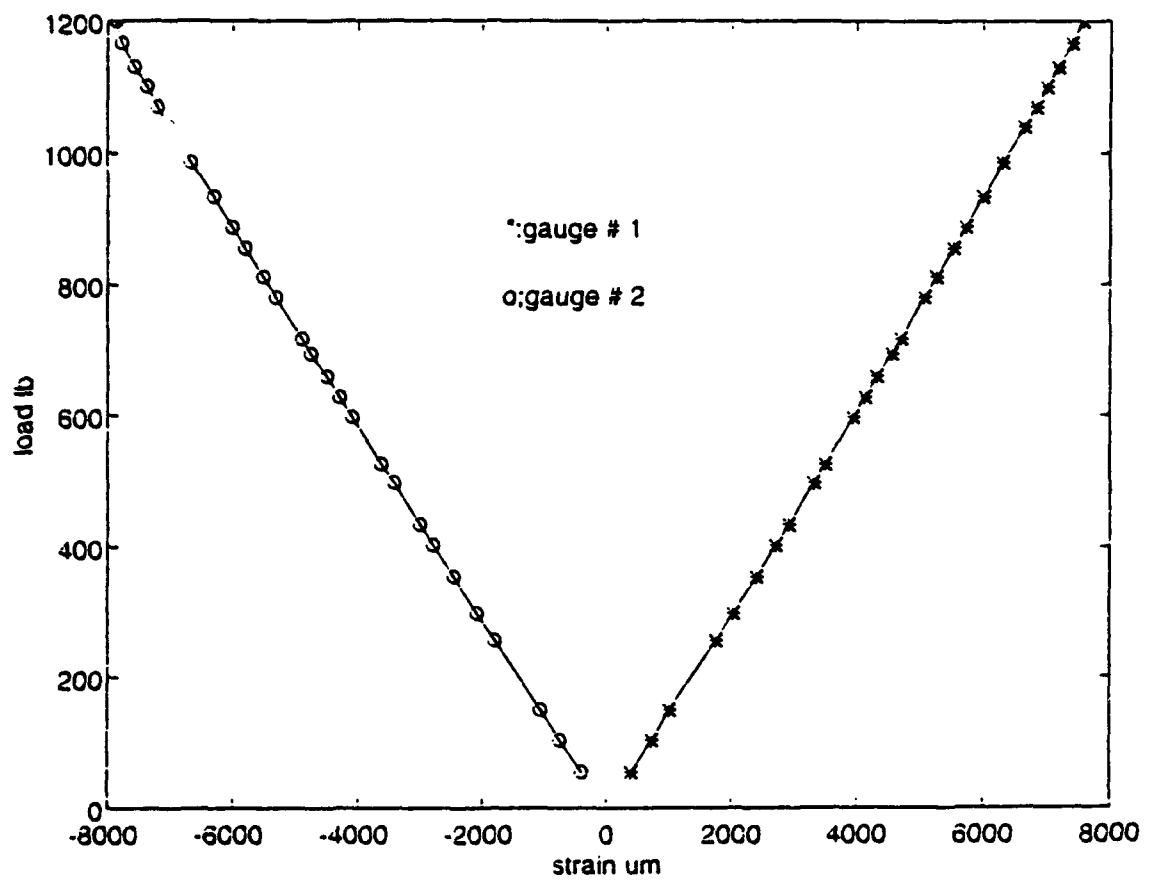


Figure 7. Stress- strain diagram for [0] laminate without a hole

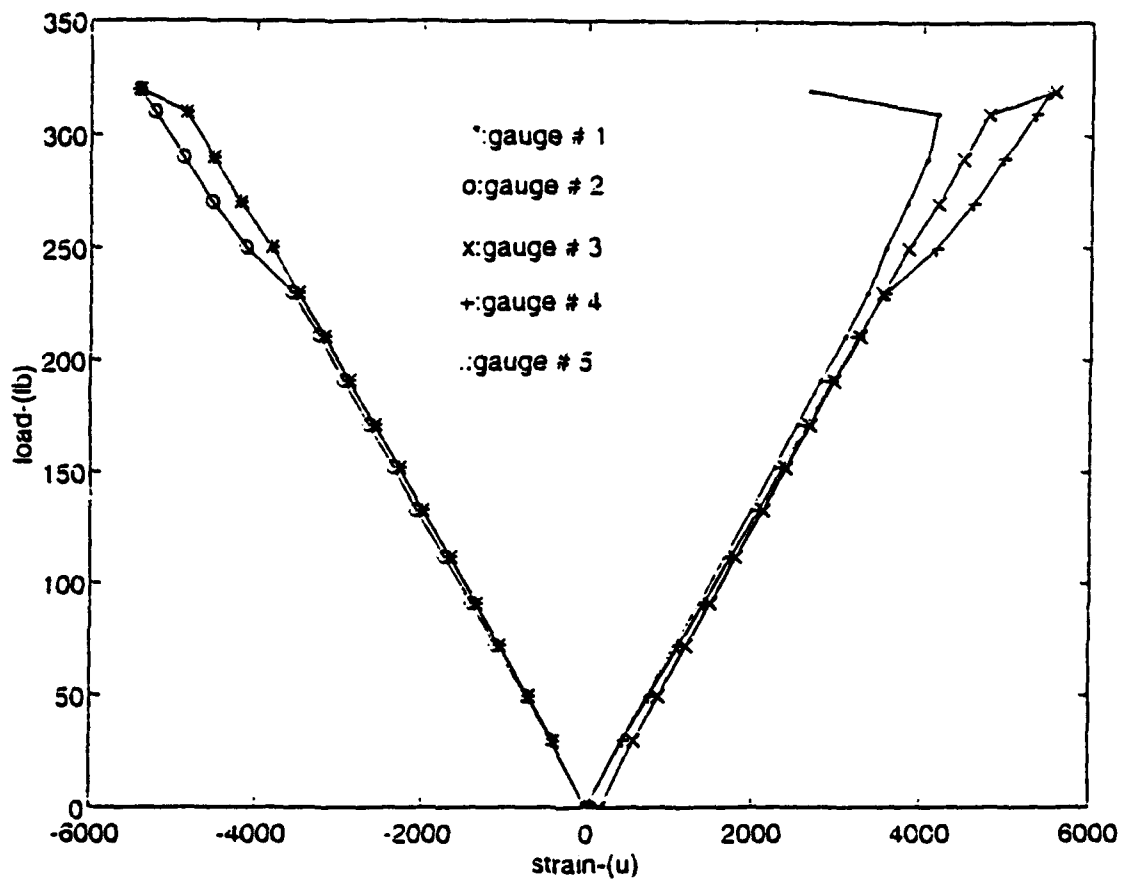


Figure 8. Stress- strain diagram for [0] laminate with
a 1/4" hole at the center

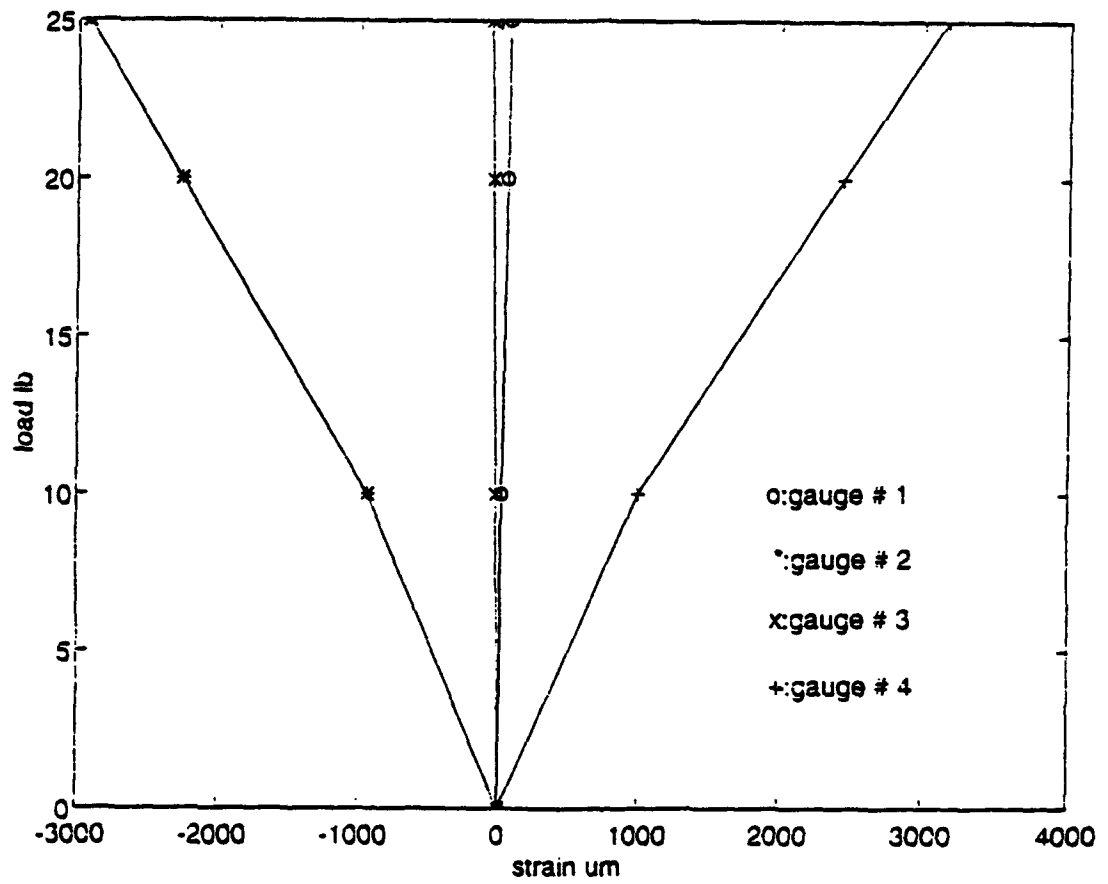


Figure 9. Stress- strain diagram for [90] laminate without a hole

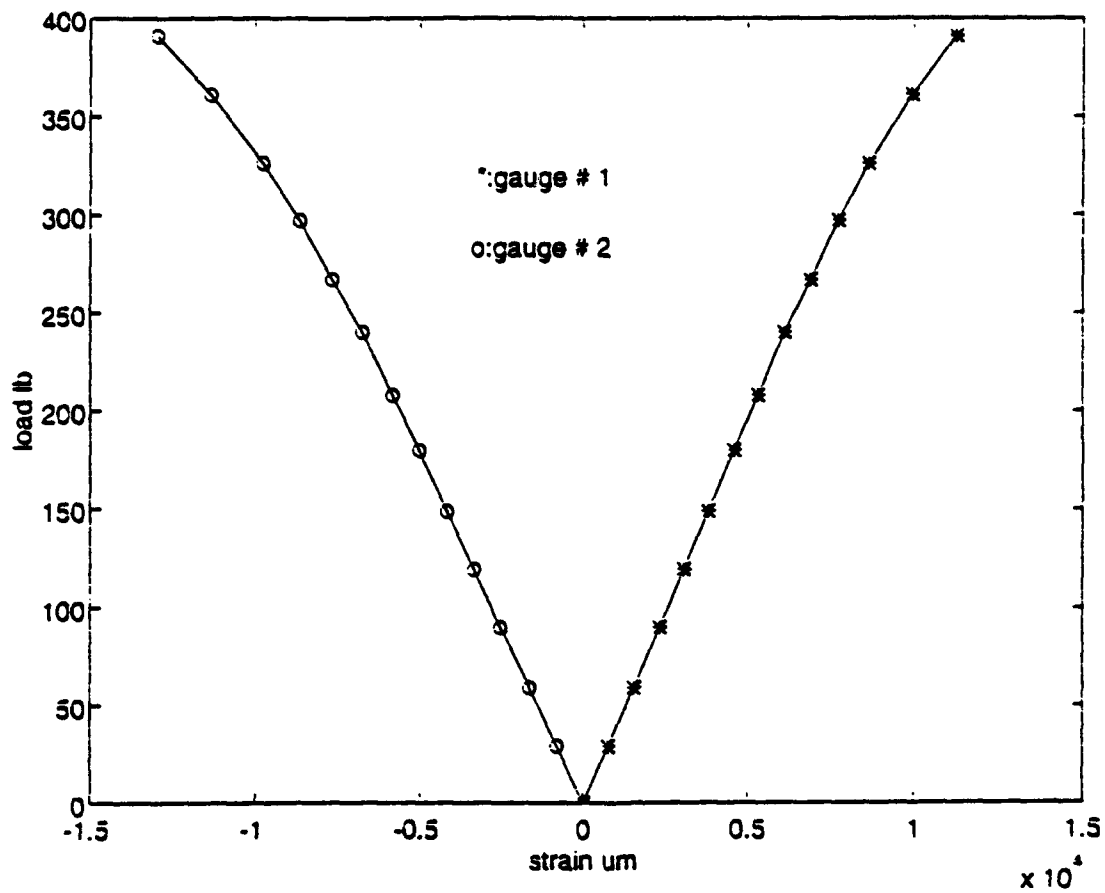


Figure 10. Stress- strain diagram for [0/90] laminate without a hole

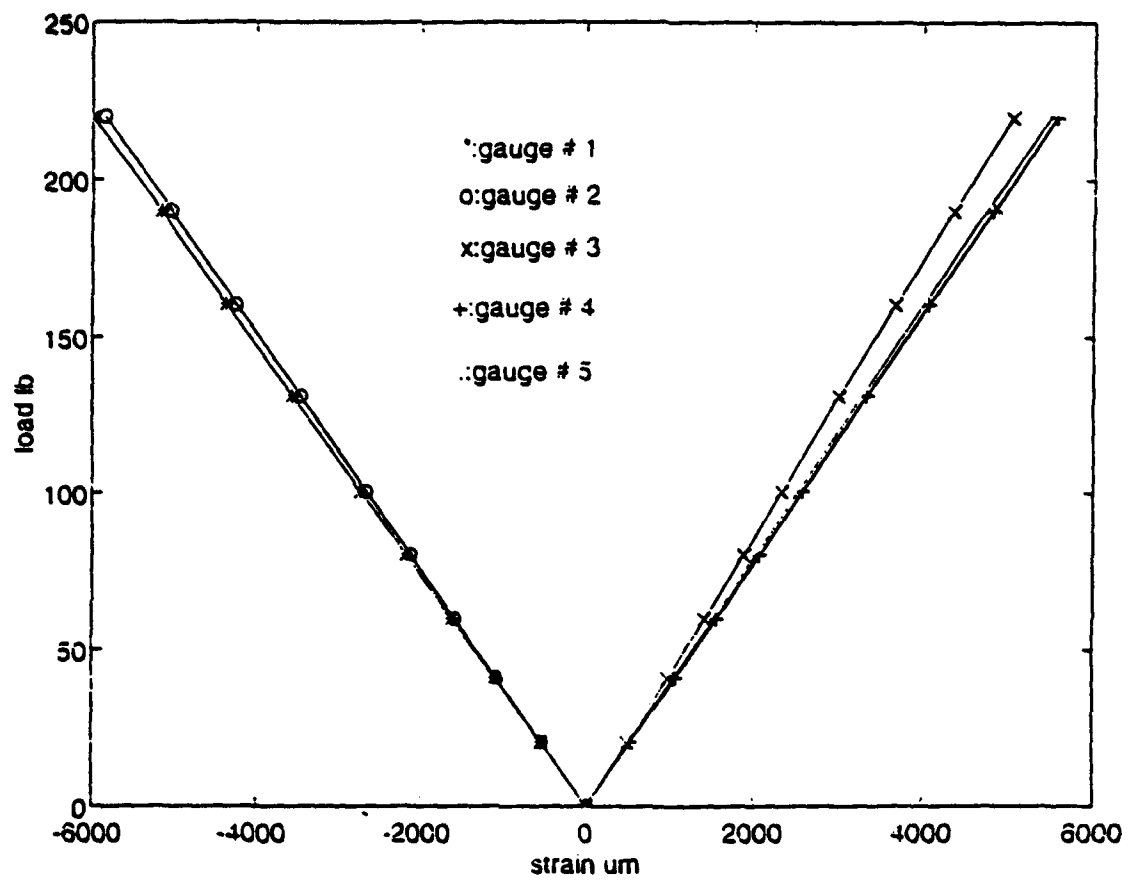


Figure 11. Stress- strain diagram for [0/90] laminate with a 1/4" hole at the center

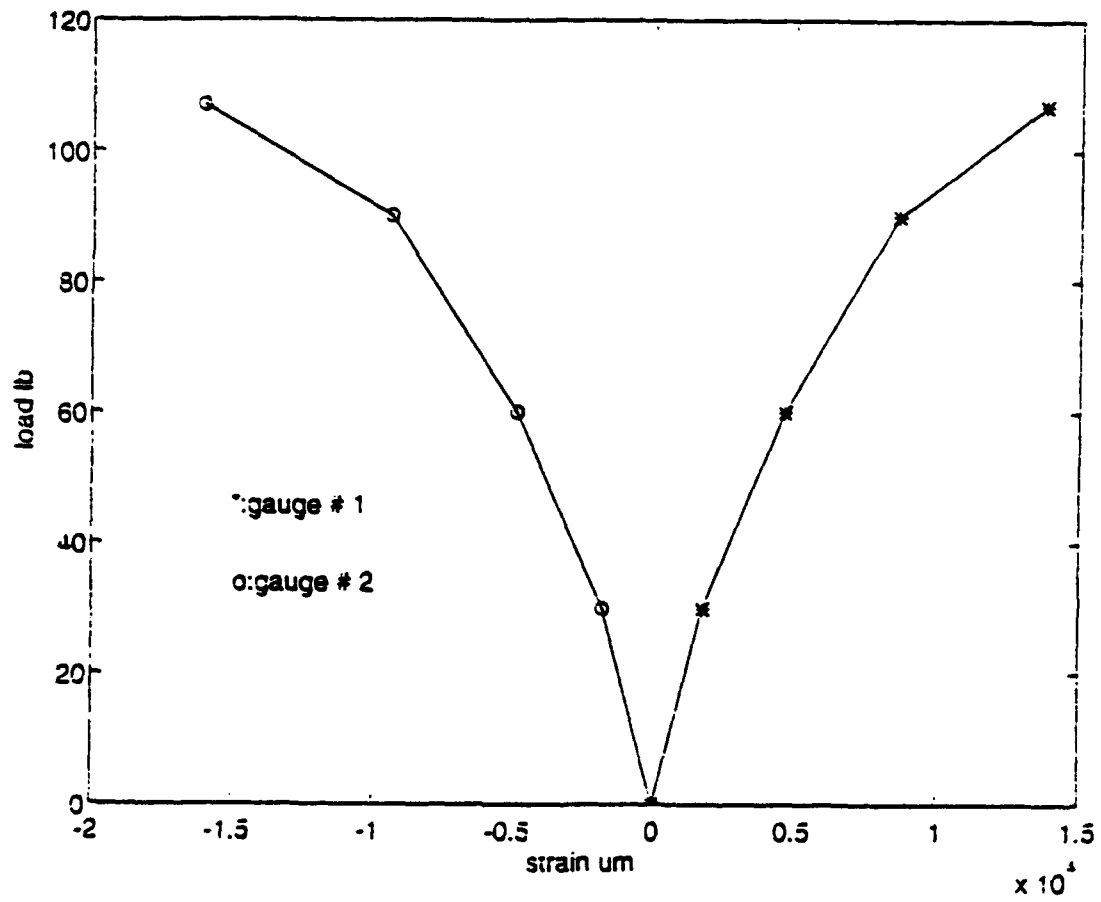


Figure 12. Stress- strain diagram for $[+45/-45]$ laminate without a hole

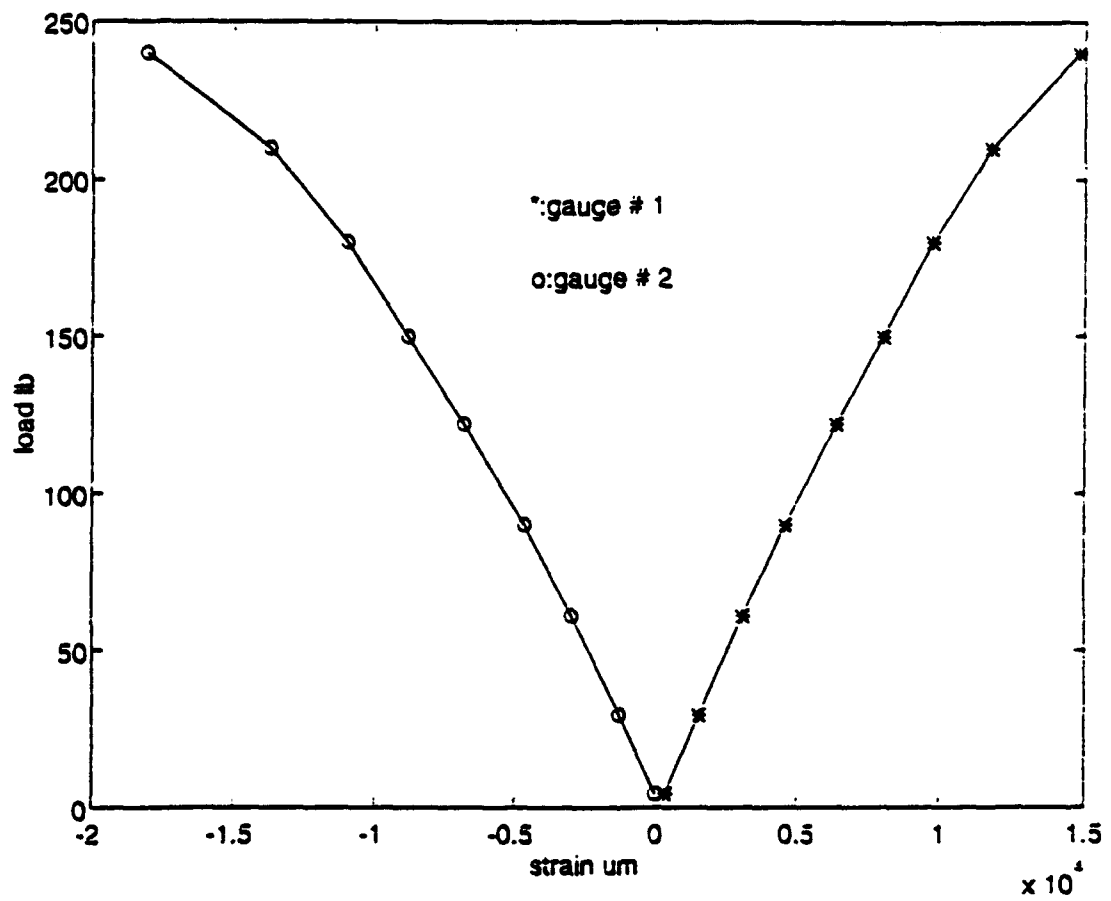


Figure 13. Stress- strain diagram for $[+45/-45]$ laminate without a hole

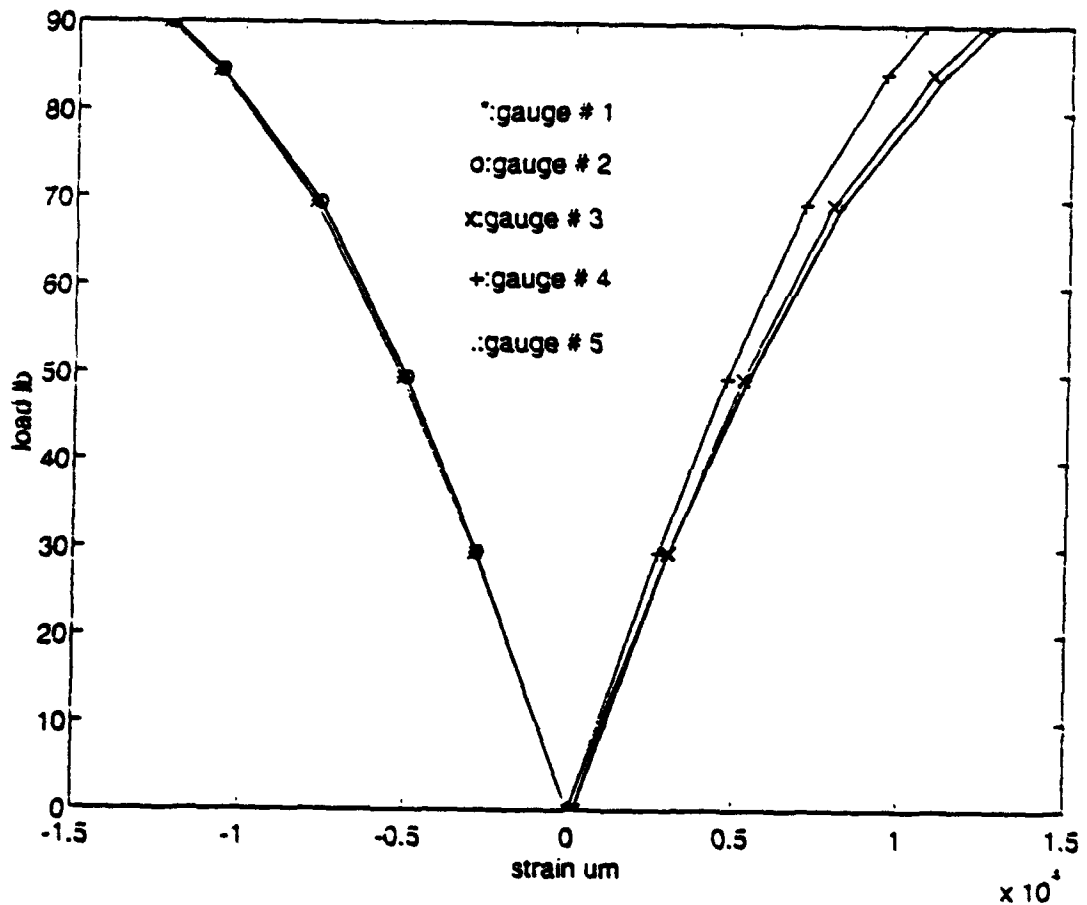


Figure 14. Stress- strain diagram for $[+45/-45]$ laminate with a $1/4"$ hole at the center

V. FINITE ELEMENT ANALYSIS

A. OVERVIEW

Since the earliest development of the finite element method, a large of plate bending elements have been developed and reported in the literature. For example, Batoz et al. [Ref. 10], with the purpose of identifying the most effective element for the thin plate analysis, presented an assessment of flat triangular plate bending elements with displacement degrees-of-freedom at the three corner nodes only. They claimed that the most efficient and reliable three-node plate bending elements were based on the discrete Kirchhoff theory and a hybrid stress model. Later on, he [Ref. 11] also presented the explicit expression of the stiffness matrix of the nine degree-of-freedom plate bending triangular element (called discrete Kirchhoff triangle) which allowed, as he said, a significant reduction of algebraic operations in the evaluation of the stiffness matrices and bending moments.

In 1983, Fricker [Ref. 12], based on Razzaque's report, described a new three-noded triangular element for plate bending with an extra internal 'bubble' function proposed by Irons for making the Razzaque's element more

flexible. He also claimed that his element and that developed by Hansen, Bergan, and Syvertsen were the two most accurate triangular thin plate elements currently available. Furthermore, Lee and Zhang [Ref.13] developed a six-node plate bending element based on a modified Hellinger-Reissener principle and the Reissner-Mindlin plate bending theory to obtain more accurate and reliable solution.

In this thesis, a triangular plate bending element, which was developed by Tocher[Ref. 15], is used to analyze the laminated composite plates subjected to a pure bending load and to determine the deflections, strains, and stresses of the plates.

B. TRIANGULAR PLATE BENDING ELEMENT FORMULATION

The plate, in general, may have any irregular geometry and loading. The derivations are based on assumptions of the small deformation theory, described in the earlier chapter. A triangular plate element is employed for the following development. Each nodal displacement of the element possesses three components: a displacement in the z direction, w ; a rotation about the x axis, w_y (derivative of w with respect to y); and a rotation about

the y axis, w_x (derivative of w with respect to x), as shown in Figure 15. The displacement function, w , is assumed to be

$$w(x, y) = a_1 + a_2x + a_3y + a_4x^2 + a_5xy + a_6y^2 + a_7x^3 + a_8(x^2y + xy^2) + a_9y^3 + a_{10}x^4 + a_{11}x^2y^2 + a_{12}y^4 + a_{13}x^5 + a_{14}x^3y^2 + a_{15}x^2y^3 + a_{16}y^5 + a_{17}x^6 + a_{18}x^4y^2 + a_{19}x^2y^4 + a_{20}y^6 + a_{21}x^7 + a_{22}x^5y^2 + a_{23}x^3y^4 + a_{24}x^2y^5 + a_{25}y^7 + a_{26}x^8 + a_{27}x^6y^2 + a_{28}x^4y^4 + a_{29}x^2y^6 + a_{30}y^8 + a_{31}x^9 + a_{32}x^7y^2 + a_{33}x^5y^4 + a_{34}x^3y^6 + a_{35}x^2y^8 + a_{36}y^9 + a_{37}x^{10} + a_{38}x^8y^2 + a_{39}x^6y^4 + a_{40}x^4y^6 + a_{41}x^2y^8 + a_{42}y^{10} + a_{43}x^{11} + a_{44}x^9y^2 + a_{45}x^7y^4 + a_{46}x^5y^6 + a_{47}x^3y^8 + a_{48}x^2y^{10} + a_{49}y^{11} + a_{50}x^{12} + a_{51}x^{10}y^2 + a_{52}x^8y^4 + a_{53}x^6y^6 + a_{54}x^4y^8 + a_{55}x^2y^{10} + a_{56}y^{12} + a_{57}x^{13} + a_{58}x^{11}y^2 + a_{59}x^9y^4 + a_{60}x^7y^6 + a_{61}x^5y^8 + a_{62}x^3y^{10} + a_{63}x^2y^{12} + a_{64}y^{13} + a_{65}x^{14} + a_{66}x^{12}y^2 + a_{67}x^{10}y^4 + a_{68}x^8y^6 + a_{69}x^6y^8 + a_{70}x^4y^{10} + a_{71}x^2y^{12} + a_{72}y^{14} + a_{73}x^{15} + a_{74}x^{13}y^2 + a_{75}x^{11}y^4 + a_{76}x^9y^6 + a_{77}x^7y^8 + a_{78}x^5y^{10} + a_{79}x^3y^{12} + a_{80}x^2y^{14} + a_{81}y^{15} + a_{82}x^{16} + a_{83}x^{14}y^2 + a_{84}x^{12}y^4 + a_{85}x^{10}y^6 + a_{86}x^8y^8 + a_{87}x^6y^{10} + a_{88}x^4y^{12} + a_{89}x^2y^{14} + a_{90}y^{16} + a_{91}x^{17} + a_{92}x^{15}y^2 + a_{93}x^{13}y^4 + a_{94}x^{11}y^6 + a_{95}x^9y^8 + a_{96}x^7y^{10} + a_{97}x^5y^{12} + a_{98}x^3y^{14} + a_{99}x^2y^{16} + a_{100}y^{17} + a_{101}x^{18} + a_{102}x^{16}y^2 + a_{103}x^{14}y^4 + a_{104}x^{12}y^6 + a_{105}x^{10}y^8 + a_{106}x^8y^{10} + a_{107}x^6y^{12} + a_{108}x^4y^{14} + a_{109}x^2y^{16} + a_{110}y^{18} + a_{111}x^{19} + a_{112}x^{17}y^2 + a_{113}x^{15}y^4 + a_{114}x^{13}y^6 + a_{115}x^{11}y^8 + a_{116}x^9y^{10} + a_{117}x^7y^{12} + a_{118}x^5y^{14} + a_{119}x^3y^{16} + a_{120}x^2y^{18} + a_{121}y^{19} + a_{122}x^{20} + a_{123}x^{18}y^2 + a_{124}x^{16}y^4 + a_{125}x^{14}y^6 + a_{126}x^{12}y^8 + a_{127}x^{10}y^{10} + a_{128}x^8y^{12} + a_{129}x^6y^{14} + a_{130}x^4y^{16} + a_{131}x^2y^{18} + a_{132}y^{20} + a_{133}x^{21} + a_{134}x^{19}y^2 + a_{135}x^{17}y^4 + a_{136}x^{15}y^6 + a_{137}x^{13}y^8 + a_{138}x^{11}y^{10} + a_{139}x^9y^{12} + a_{140}x^7y^{14} + a_{141}x^5y^{16} + a_{142}x^3y^{18} + a_{143}x^2y^{20} + a_{144}y^{21} + a_{145}x^{22} + a_{146}x^{20}y^2 + a_{147}x^{18}y^4 + a_{148}x^{16}y^6 + a_{149}x^{14}y^8 + a_{150}x^{12}y^{10} + a_{151}x^{10}y^{12} + a_{152}x^8y^{14} + a_{153}x^6y^{16} + a_{154}x^4y^{18} + a_{155}x^2y^{20} + a_{156}y^{22} + a_{157}x^{23} + a_{158}x^{21}y^2 + a_{159}x^{19}y^4 + a_{160}x^{17}y^6 + a_{161}x^{15}y^8 + a_{162}x^{13}y^{10} + a_{163}x^{11}y^{12} + a_{164}x^9y^{14} + a_{165}x^7y^{16} + a_{166}x^5y^{18} + a_{167}x^3y^{20} + a_{168}x^2y^{22} + a_{169}y^{23} + a_{170}x^{24} + a_{171}x^{22}y^2 + a_{172}x^{20}y^4 + a_{173}x^{18}y^6 + a_{174}x^{16}y^8 + a_{175}x^{14}y^{10} + a_{176}x^{12}y^{12} + a_{177}x^{10}y^{14} + a_{178}x^8y^{16} + a_{179}x^6y^{18} + a_{180}x^4y^{20} + a_{181}x^2y^{22} + a_{182}y^{24} + a_{183}x^{25} + a_{184}x^{23}y^2 + a_{185}x^{21}y^4 + a_{186}x^{19}y^6 + a_{187}x^{17}y^8 + a_{188}x^{15}y^{10} + a_{189}x^{13}y^{12} + a_{190}x^{11}y^{14} + a_{191}x^9y^{16} + a_{192}x^7y^{18} + a_{193}x^5y^{20} + a_{194}x^3y^{22} + a_{195}x^2y^{24} + a_{196}y^{25} + a_{197}x^{26} + a_{198}x^{24}y^2 + a_{199}x^{22}y^4 + a_{200}x^{20}y^6 + a_{201}x^{18}y^8 + a_{202}x^{16}y^{10} + a_{203}x^{14}y^{12} + a_{204}x^{12}y^{14} + a_{205}x^{10}y^{16} + a_{206}x^8y^{18} + a_{207}x^6y^{20} + a_{208}x^4y^{22} + a_{209}x^2y^{24} + a_{210}y^{26} + a_{211}x^{27} + a_{212}x^{25}y^2 + a_{213}x^{23}y^4 + a_{214}x^{21}y^6 + a_{215}x^{19}y^8 + a_{216}x^{17}y^{10} + a_{217}x^{15}y^{12} + a_{218}x^{13}y^{14} + a_{219}x^{11}y^{16} + a_{220}x^9y^{18} + a_{221}x^7y^{20} + a_{222}x^5y^{22} + a_{223}x^3y^{24} + a_{224}x^2y^{26} + a_{225}y^{27} + a_{226}x^{28} + a_{227}x^{26}y^2 + a_{228}x^{24}y^4 + a_{229}x^{22}y^6 + a_{230}x^{20}y^8 + a_{231}x^{18}y^{10} + a_{232}x^{16}y^{12} + a_{233}x^{14}y^{14} + a_{234}x^{12}y^{16} + a_{235}x^{10}y^{18} + a_{236}x^8y^{20} + a_{237}x^6y^{22} + a_{238}x^4y^{24} + a_{239}x^2y^{26} + a_{240}y^{28} + a_{241}x^{29} + a_{242}x^{27}y^2 + a_{243}x^{25}y^4 + a_{244}x^{23}y^6 + a_{245}x^{21}y^8 + a_{246}x^{19}y^{10} + a_{247}x^{17}y^{12} + a_{248}x^{15}y^{14} + a_{249}x^{13}y^{16} + a_{250}x^{11}y^{18} + a_{251}x^9y^{20} + a_{252}x^7y^{22} + a_{253}x^5y^{24} + a_{254}x^3y^{26} + a_{255}x^2y^{28} + a_{256}y^{29} + a_{257}x^{30} + a_{258}x^{28}y^2 + a_{259}x^{26}y^4 + a_{260}x^{24}y^6 + a_{261}x^{22}y^8 + a_{262}x^{20}y^{10} + a_{263}x^{18}y^{12} + a_{264}x^{16}y^{14} + a_{265}x^{14}y^{16} + a_{266}x^{12}y^{18} + a_{267}x^{10}y^{20} + a_{268}x^8y^{22} + a_{269}x^6y^{24} + a_{270}x^4y^{26} + a_{271}x^2y^{28} + a_{272}y^{30} + a_{273}x^{31} + a_{274}x^{29}y^2 + a_{275}x^{27}y^4 + a_{276}x^{25}y^6 + a_{277}x^{23}y^8 + a_{278}x^{21}y^{10} + a_{279}x^{19}y^{12} + a_{280}x^{17}y^{14} + a_{281}x^{15}y^{16} + a_{282}x^{13}y^{18} + a_{283}x^{11}y^{20} + a_{284}x^9y^{22} + a_{285}x^7y^{24} + a_{286}x^5y^{26} + a_{287}x^3y^{28} + a_{288}x^2y^{30} + a_{289}y^{31} + a_{290}x^{32} + a_{291}x^{30}y^2 + a_{292}x^{28}y^4 + a_{293}x^{26}y^6 + a_{294}x^{24}y^8 + a_{295}x^{22}y^{10} + a_{296}x^{20}y^{12} + a_{297}x^{18}y^{14} + a_{298}x^{16}y^{16} + a_{299}x^{14}y^{18} + a_{300}x^{12}y^{20} + a_{301}x^{10}y^{22} + a_{302}x^8y^{24} + a_{303}x^6y^{26} + a_{304}x^4y^{28} + a_{305}x^2y^{30} + a_{306}y^{32} + a_{307}x^{33} + a_{308}x^{31}y^2 + a_{309}x^{29}y^4 + a_{310}x^{27}y^6 + a_{311}x^{25}y^8 + a_{312}x^{23}y^{10} + a_{313}x^{21}y^{12} + a_{314}x^{19}y^{14} + a_{315}x^{17}y^{16} + a_{316}x^{15}y^{18} + a_{317}x^{13}y^{20} + a_{318}x^{11}y^{22} + a_{319}x^9y^{24} + a_{320}x^7y^{26} + a_{321}x^5y^{28} + a_{322}x^3y^{30} + a_{323}x^2y^{32} + a_{324}y^{33} + a_{325}x^{34} + a_{326}x^{32}y^2 + a_{327}x^{30}y^4 + a_{328}x^{28}y^6 + a_{329}x^{26}y^8 + a_{330}x^{24}y^{10} + a_{331}x^{22}y^{12} + a_{332}x^{20}y^{14} + a_{333}x^{18}y^{16} + a_{334}x^{16}y^{18} + a_{335}x^{14}y^{20} + a_{336}x^{12}y^{22} + a_{337}x^{10}y^{24} + a_{338}x^8y^{26} + a_{339}x^6y^{28} + a_{340}x^4y^{30} + a_{341}x^2y^{32} + a_{342}y^{34} + a_{343}x^{35} + a_{344}x^{33}y^2 + a_{345}x^{31}y^4 + a_{346}x^{29}y^6 + a_{347}x^{27}y^8 + a_{348}x^{25}y^{10} + a_{349}x^{23}y^{12} + a_{350}x^{21}y^{14} + a_{351}x^{19}y^{16} + a_{352}x^{17}y^{18} + a_{353}x^{15}y^{20} + a_{354}x^{13}y^{22} + a_{355}x^{11}y^{24} + a_{356}x^9y^{26} + a_{357}x^7y^{28} + a_{358}x^5y^{30} + a_{359}x^3y^{32} + a_{360}x^2y^{34} + a_{361}y^{35} + a_{362}x^{36} + a_{363}x^{34}y^2 + a_{364}x^{32}y^4 + a_{365}x^{30}y^6 + a_{366}x^{28}y^8 + a_{367}x^{26}y^{10} + a_{368}x^{24}y^{12} + a_{369}x^{22}y^{14} + a_{370}x^{20}y^{16} + a_{371}x^{18}y^{18} + a_{372}x^{16}y^{20} + a_{373}x^{14}y^{22} + a_{374}x^{12}y^{24} + a_{375}x^{10}y^{26} + a_{376}x^8y^{28} + a_{377}x^6y^{30} + a_{378}x^4y^{32} + a_{379}x^2y^{34} + a_{380}y^{36} + a_{381}x^{37} + a_{382}x^{35}y^2 + a_{383}x^{33}y^4 + a_{384}x^{31}y^6 + a_{385}x^{29}y^8 + a_{386}x^{27}y^{10} + a_{387}x^{25}y^{12} + a_{388}x^{23}y^{14} + a_{389}x^{21}y^{16} + a_{390}x^{19}y^{18} + a_{391}x^{17}y^{20} + a_{392}x^{15}y^{22} + a_{393}x^{13}y^{24} + a_{394}x^{11}y^{26} + a_{395}x^9y^{28} + a_{396}x^7y^{30} + a_{397}x^5y^{32} + a_{398}x^3y^{34} + a_{399}x^2y^{36} + a_{400}y^{37} + a_{401}x^{40} + a_{402}x^{38}y^2 + a_{403}x^{36}y^4 + a_{404}x^{34}y^6 + a_{405}x^{32}y^8 + a_{406}x^{30}y^{10} + a_{407}x^{28}y^{12} + a_{408}x^{26}y^{14} + a_{409}x^{24}y^{16} + a_{410}x^{22}y^{18} + a_{411}x^{20}y^{20} + a_{412}x^{18}y^{22} + a_{413}x^{16}y^{24} + a_{414}x^{14}y^{26} + a_{415}x^{12}y^{28} + a_{416}x^{10}y^{30} + a_{417}x^8y^{32} + a_{418}x^6y^{34} + a_{419}x^4y^{36} + a_{420}x^2y^{38} + a_{421}y^{40} + a_{422}x^{41} + a_{423}x^{39}y^2 + a_{424}x^{37}y^4 + a_{425}x^{35}y^6 + a_{426}x^{33}y^8 + a_{427}x^{31}y^{10} + a_{428}x^{29}y^{12} + a_{429}x^{27}y^{14} + a_{430}x^{25}y^{16} + a_{431}x^{23}y^{18} + a_{432}x^{21}y^{20} + a_{433}x^{19}y^{22} + a_{434}x^{17}y^{24} + a_{435}x^{15}y^{26} + a_{436}x^{13}y^{28} + a_{437}x^{11}y^{30} + a_{438}x^9y^{32} + a_{439}x^7y^{34} + a_{440}x^5y^{36} + a_{441}x^3y^{38} + a_{442}x^2y^{40} + a_{443}y^{41} + a_{444}x^{42} + a_{445}x^{40}y^2 + a_{446}x^{38}y^4 + a_{447}x^{36}y^6 + a_{448}x^{34}y^8 + a_{449}x^{32}y^{10} + a_{450}x^{30}y^{12} + a_{451}x^{28}y^{14} + a_{452}x^{26}y^{16} + a_{453}x^{24}y^{18} + a_{454}x^{22}y^{20} + a_{455}x^{20}y^{22} + a_{456}x^{18}y^{24} + a_{457}x^{16}y^{26} + a_{458}x^{14}y^{28} + a_{459}x^{12}y^{30} + a_{460}x^{10}y^{32} + a_{461}x^8y^{34} + a_{462}x^6y^{36} + a_{463}x^4y^{38} + a_{464}x^2y^{40} + a_{465}y^{42} + a_{466}x^{43} + a_{467}x^{41}y^2 + a_{468}x^{39}y^4 + a_{469}x^{37}y^6 + a_{470}x^{35}y^8 + a_{471}x^{33}y^{10} + a_{472}x^{31}y^{12} + a_{473}x^{29}y^{14} + a_{474}x^{27}y^{16} + a_{475}x^{25}y^{18} + a_{476}x^{23}y^{20} + a_{477}x^{21}y^{22} + a_{478}x^{19}y^{24} + a_{479}x^{17}y^{26} + a_{480}x^{15}y^{28} + a_{481}x^{13}y^{30} + a_{482}x^{11}y^{32} + a_{483}x^9y^{34} + a_{484}x^7y^{36} + a_{485}x^5y^{38} + a_{486}x^3y^{40} + a_{487}x^2y^{42} + a_{488}y^{43} + a_{489}x^{44} + a_{490}x^{42}y^2 + a_{491}x^{40}y^4 + a_{492}x^{38}y^6 + a_{493}x^{36}y^8 + a_{494}x^{34}y^{10} + a_{495}x^{32}y^{12} + a_{496}x^{30}y^{14} + a_{497}x^{28}y^{16} + a_{498}x^{26}y^{18} + a_{499}x^{24}y^{20} + a_{500}x^{22}y^{22} + a_{501}x^{20}y^{24} + a_{502}x^{18}y^{26} + a_{503}x^{16}y^{28} + a_{504}x^{14}y^{30} + a_{505}x^{12}y^{32} + a_{506}x^{10}y^{34} + a_{507}x^8y^{36} + a_{508}x^6y^{38} + a_{509}x^4y^{40} + a_{510}x^2y^{42} + a_{511}y^{44} + a_{512}x^{45} + a_{513}x^{43}y^2 + a_{514}x^{41}y^4 + a_{515}x^{39}y^6 + a_{516}x^{37}y^8 + a_{517}x^{35}y^{10} + a_{518}x^{33}y^{12} + a_{519}x^{31}y^{14} + a_{520}x^{29}y^{16} + a_{521}x^{27}y^{18} + a_{522}x^{25}y^{20} + a_{523}x^{23}y^{22} + a_{524}x^{21}y^{24} + a_{525}x^{19}y^{26} + a_{526}x^{17}y^{28} + a_{527}x^{15}y^{30} + a_{528}x^{13}y^{32} + a_{529}x^{11}y^{34} + a_{530}x^9y^{36} + a_{531}x^7y^{38} + a_{532}x^5y^{40} + a_{533}x^3y^{42} + a_{534}x^2y^{44} + a_{535}y^{45} + a_{536}x^{46} + a_{537}x^{44}y^2 + a_{538}x^{42}y^4 + a_{539}x^{40}y^6 + a_{540}x^{38}y^8 + a_{541}x^{36}y^{10} + a_{542}x^{34}y^{12} + a_{543}x^{32}y^{14} + a_{544}x^{30}y^{16} + a_{545}x^{28}y^{18} + a_{546}x^{26}y^{20} + a_{547}x^{24}y^{22} + a_{548}x^{22}y^{24} + a_{549}x^{20}y^{26} + a_{550}x^{18}y^{28} + a_{551}x^{16}y^{30} + a_{552}x^{14}y^{32} + a_{553}x^{12}y^{34} + a_{554}x^{10}y^{36} + a_{555}x^8y^{38} + a_{556}x^6y^{40} + a_{557}x^4y^{42} + a_{558}x^2y^{44} + a_{559}y^{46} + a_{560}x^{47} + a_{561}x^{45}y^2 + a_{562}x^{43}y^4 + a_{563}x^{41}y^6 + a_{564}x^{39}y^8 + a_{565}x^{37}y^{10} + a_{566}x^{35}y^{12} + a_{567}x^{33}y^{14} + a_{568}x^{31}y^{16} + a_{569}x^{29}y^{18} + a_{570}x^{27}y^{20} + a_{571}x^{25}y^{22} + a_{572}x^{23}y^{24} + a_{573}x^{21}y^{26} + a_{574}x^{19}y^{28} + a_{575}x^{17}y^{30} + a_{576}x^{15}y^{32} + a_{577}x^{13}y^{34} + a_{578}x^{11}y^{36} + a_{579}x^9y^{38} + a_{580}x^7y^{40} + a_{581}x^5y^{42} + a_{582}x^3y^{44} + a_{583}x^2y^{46} + a_{584}y^{47} + a_{585}x^{48} + a_{586}x^{46}y^2 + a_{587}x^{44}y^4 + a_{588}x^{42}y^6 + a_{589}x^{40}y^8 + a_{590}x^{38}y^{10} + a_{591}x^{36}y^{12} + a_{592}x^{34}y^{14} + a_{593}x^{32}y^{16} + a_{594}x^{30}y^{18} + a_{595}x^{28}y^{20} + a_{596}x^{26}y^{22} + a_{597}x^{24}y^{24} + a_{598}x^{22}y^{26} + a_{599}x^{20}y^{28} + a_{600}x^{18}y^{30} + a_{601}x^{16}y^{32} + a_{602}x^{14}y^{34} + a_{603}x^{12}y^{36} + a_{604}x^{10}y^{38} + a_{605}x^8y^{40} + a_{606}x^6y^{42} + a_{607}x^4y^{44} + a_{608}x^2y^{46} + a_{609}y^{48} + a_{610}x^{49} + a_{611}x^{47}y^2 + a_{612}x^{45}y^4 + a_{613}x^{43}y^6 + a_{614}x^{41}y^8 + a_{615}x^{39}y^{10} + a_{616}x^{37}y^{12} + a_{617}x^{35}y^{14} + a_{618}x^{33}y^{16} + a_{619}x^{31}y^{18} + a_{620}x^{29}y^{20} + a_{621}x^{27}y^{22} + a_{622}x^{25}y^{24} + a_{623}x^{23}y^{26} + a_{624}x^{21}y^{28} + a_{625}x^{19}y^{30} + a_{626}x^{17}y^{32} + a_{627}x^{15}y^{34} + a_{628}x^{13}y^{36} + a_{629}x^{11}y^{38} + a_{630}x^9y^{40} + a_{631}x^7y^{42} + a_{632}x^5y^{44} + a_{633}x^3y^{46} + a_{634}x^2y^{48} + a_{635}y^{49} + a_{636}x^{50} + a_{637}x^{48}y^2 + a_{638}x^{46}y^4 + a_{639}x^{44}y^6 + a_{640}x^{42}y^8 + a_{641}x^{40}y^{10} + a_{642}x^{38}y^{12} + a_{643}x^{36}y^{14} + a_{644}x^{34}y^{16} + a_{645}x^{32}y^{18} + a_{646}x^{30}y^{20} + a_{647}x^{28}y^{22} + a_{648}x^{26}y^{24} + a_{649}x^{24}y^{26} + a_{650}x^{22}y^{28} + a_{651}x^{20}y^{30} + a_{652}x^{18}y^{32} + a_{653}x^{16}y^{34} + a_{654}x^{14}y^{36} + a_{655}x^{12}y^{38} + a_{656}x^{10}y^{40} + a_{657}x^8y^{42} + a_{658}x^6y^{44} + a_{659}x^4y^{46} + a_{660}x^2y^{48} + a_{661}y^{50} + a_{662}x^{51} + a_{663}x^{49}y^2 + a_{664}x^{47}y^4 + a_{665}x^{45}y^6 + a_{666}x^{43}y^8 + a_{667}x^{41}y^{10} + a_{668}x^{39}y^{12} + a_{669}x^{37}y^{14} + a_{670}x^{35}y^{16} + a_{671}x^{33}y^{18} + a_{672}x^{31}y^{20} + a_{673}x^{29}y^{22} + a_{674}x^{27}y^{24} + a_{675}x^{25}y^{26} + a_{676}x^{23}y^{28} + a_{677}x^{21}y^{30} + a_{678}x^{19}y^{32} + a_{679}x^{17}y^{34} + a_{680}x^{15}y^{36} + a_{681}x^{13}y^{38} + a_{682}x^{11}y^{40} + a_{683}x^9y^{42} + a_{684}x^7y^{44} + a_{685}x^5y^{46} + a_{686}x^3y^{48} + a_{687}x^2y^{50} + a_{688}y^{51} + a_{689}x^{52} + a_{690}x^{50}y^2 + a_{691}x^{48}y^4 + a_{692}x^{46}y^6 + a_{693}x^{44}y^8 + a_{694}x^{42}y^{10} + a_{695}x^{40}y^{12} + a_{696}x^{38}y^{14} + a_{697}x^{36}y^{16} + a_{698}x^{34}y^{18} + a_{699}x^{32}y^{20} + a_{700}x^{30}y^{22} + a_{701}x^{28}y^{24} + a_{702}x^{26}y^{26} + a_{703}x^{24}y^{28} + a_{704}x^{22}y^{30} + a_{705}x^{20}y^{32} + a_{706}x^{18}y^{34} + a_{707}x^{16}y^{36} + a_{708}x^{14}y^{38} + a_{709}x^{12}y^{40} + a_{710}x^{10}y^{42} + a_{711}x^8y^{44} + a_{712}x^6y^{46} + a_{713}x^4y^{48} + a_{714}x^2y^{50} + a_{715}y^{52} + a_{716}x^{53} + a_{717}x^{51}y^2 + a_{718}x^{49}y^4 + a_{719}x^{47}y^6 + a_{720}x^{45}y^8 + a_{721}x^{43}y^{10} + a_{722}x^{41}y^{12} + a_{723}x^{39}y^{14} + a_{724}x^{37}y^{16} + a_{725}x^{35}y^{18} + a_{726}x^{33}y^{20} + a_{727}x^{31}y^{22} + a_{728}x^{29}y^{24} + a_{729}x^{27}y^{26} + a_{730}x^{25}y^{28} + a_{731}x^{23}y^{30} + a_{732}x^{21}y^{32} + a_{733}x^{19}y^{34} + a_{734}x^{17}y^{36} + a_{735}x^{15}y^{38} + a_{736}x^{13}y^{40} + a_{737}x^{11}y^{42} + a_{738}x^9y^{44} + a_{739}x^7y^{46} + a_{740}x^5y^{48} + a_{741}x^3y^{50} + a_{742}x^2y^{52} + a_{743}y^{53} + a_{744}x^{54} + a_{745}x^{52}y^2 + a_{746}x^{50}y^4 + a_{747}x^{48}y^6 + a_{748}x^{46}y^8 + a_{749}x^{44}y^{10} + a_{750}x^{42}y^{12} + a_{751}x^{40}y^{14} + a_{752}x^{38}y^{16} + a_{753}x^{36}y^{18} + a_{754}x^{34}y^{20} + a_{755}x^{32}y^{22} + a_{756}x^{30}y^{24} + a_{757}x^{28}y^{26} + a_{758}x^{26}y^{28} + a_{759}x^{24}y^{30} + a_{760}x^{22}y^{32} + a_{761}x^{20}y^{34} + a_{762}x^{18}y^{36} + a_{763}x^{16}y^{38} + a_{764}x^{14}y^{40} + a_{765}x^{12}y^{42} + a_{766}x^{10}y^{44} + a_{767}x^8y^{46} + a_{768}x^6y^{48} + a_{769}x^4y^{50} + a_{770}x^2y^{52} + a_{771}y^{54} + a_{772}x^{55} + a_{773}x^{53}y^2 + a_{774}x^{51}y^4 + a_{775}x^{49}y^6 + a_{776}x^{47}y^8 + a_{777}x^{45}y^{10} + a_{778}x^{43}y^{12} + a_{779}x^{41}y^{14} + a_{780}x^{39}y^{16} + a_{781}x^{37}y^{18} + a_{782}x^{35}y^{20} + a_{783}x^{33}y^{22} + a_{784}x^{31}y^{24} + a_{785}x^{29}y^{26} + a_{786}x^{27}y^{28} + a_{787}x^{25}y^{30} + a_{788}x^{23}y^{32} + a_{789}x^{21}y^{34} + a_{790}x^{19}y^{36} + a_{791}x^{17}y^{38} + a_{792}x^{15}y^{40} + a_{793}x^{13}y^{42} + a_{794}x^{11}y^{44} + a_{795}x^9y^{46} + a_{796}x^7y^{48} + a_{797}x^5y^{50} + a_{798}x^3y^{52} + a_{799}x^2y^{54} + a_{800}y^{55} + a_{801}x^{56} + a_{802}x^{54}y^2 + a_{803}x^{52}y^4 + a_{804}x^{50}y^6 + a_{805}x^{48}y^8 + a_{806}x^{46}y^{10} + a_{807}x^{44}y^{12} + a_{808}x^{42}y^{14} + a_{809}x^{40}y^{16} + a_{810}x^{38}y^{18} + a_{811}x^{36}y^{20} + a_{812}x^{34}y^{22} + a_{813}x^{32}y^{24} + a_{814}x^{30}y^{26} + a_{815}x^{28}y^{28} + a_{816}x^{26}y^{30}$$

where

and

Here, the constants a_1, a_2, \dots, a_n must be determined from the nodal conditions

$$w(x,y)=q_1, \quad w_y(x,y)=q_2, \quad -w_x(x,y)=q_3 \quad \text{at } (x_1, y_1) = (0,0)$$

$$w(x,y)=q_7, \quad w_y(x,y)=q_8, \quad -w_x(x,y)=q_9 \quad \text{at} \quad (x_3, y_3) = (x_3, y_3)$$

The local y axis is taken the same as the line connecting the node 1 and node 2 with the origin placed at node 1. The local x axis is taken towards node 3 as shown in Figure 16. By using Eq.(33), Eq.(36) can be shown in the matrix form as

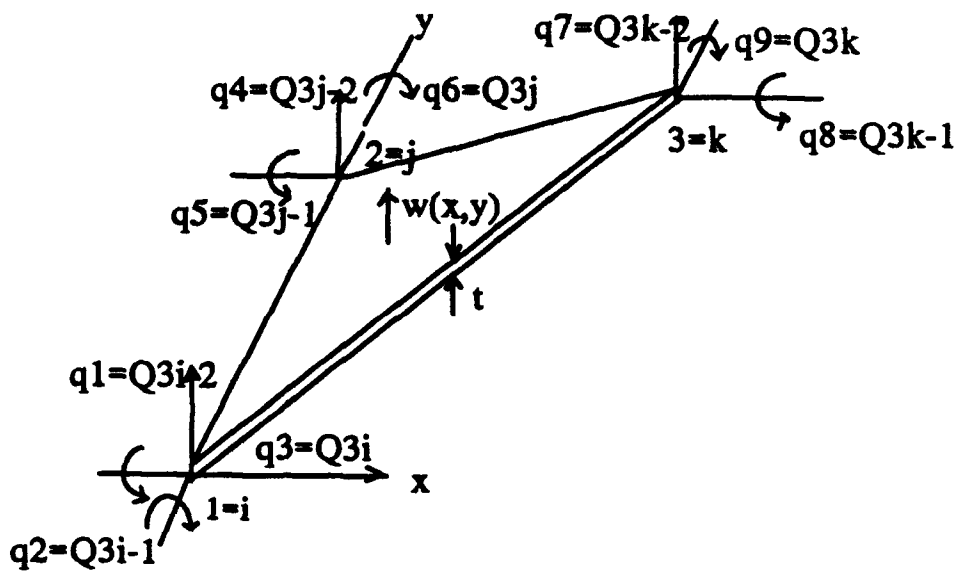


Figure 15. Nodal degrees of freedom of a triangular plate in bending

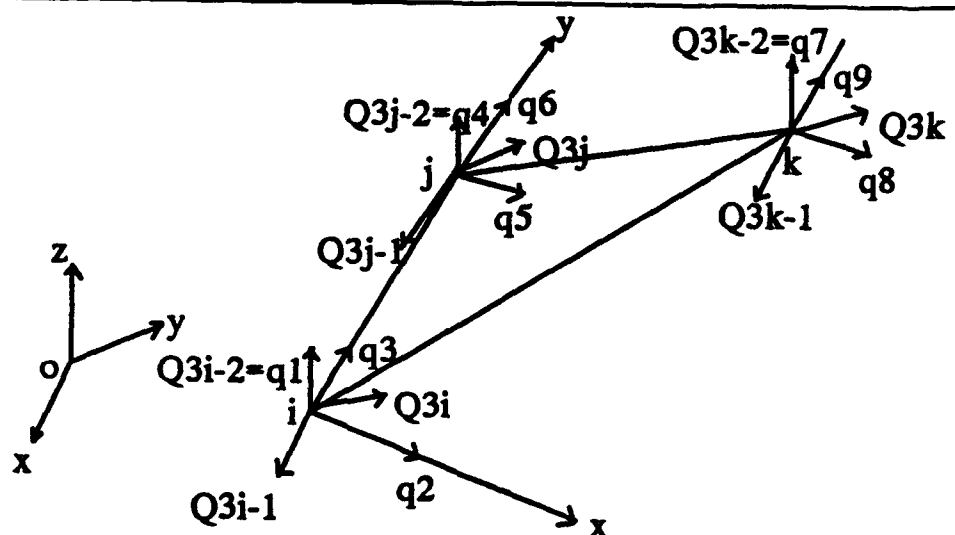


Figure 16. Local nodal coordinate system

where $[n]$ is a 9×9 matrix (see Appendix). By using Eqs.(33) and (37),

Eq.(4) can be expressed as

$$\vec{\varepsilon} = \begin{bmatrix} \tilde{H} \end{bmatrix} \vec{a} = [H] \vec{q}^{(e)} \quad \dots \dots \dots (38)$$

where

$$\left[\begin{matrix} \tilde{H} \end{matrix} \right] = -z \left[\begin{matrix} 0 & 0 & 0 & 2 & 0 & 0 & 6x & 2y & 0 \\ 0 & 0 & 0 & 0 & 0 & 2 & 0 & 2x & 6y \\ 0 & 0 & 0 & 0 & 2 & 0 & 0 & 4(x+y) & 0 \end{matrix} \right] \quad \dots \dots \dots (39)$$

and

Finally, the element stiffness matrix in the local (x,y) coordinate system can be written as

$$[K^{(e)}] = \iiint_V [H]^T [\bar{Q}] [H] dV \quad \dots \dots \dots (41)$$

where $V^{(e)}$ indicates the volume of the element and the matrix $[\bar{Q}]$ is the material property matrix for the generally orthotropic lamina. By substituting for $[H]$ from Eq.(40), Eq.(41) becomes

$$[K^{(e)}] = \left([n']^{-1} \right)^T \left[\int_{-1/2}^{1/2} dA \left(\int_{-1/2}^{1/2} \left[\tilde{H} \right]^T [Q] \left[\tilde{H} \right] dz \right) \right] [n']^{-1} \quad \dots \dots \dots (42)$$

where t is the thickness of the plate. For a laminated composite plate

$$\int_{-W/2}^{W/2} z^2 [Q] dz = \frac{1}{3} \sum_{k=1}^N [Q]_k \left(z_k^3 - z_{k-1}^3 \right) = [D] \quad \dots \dots \dots (43)$$

and the components within the bracket of Eq.(39) won't vary with the thickness. The element stiffness matrix in the local (x,y) coordinate can be rewritten as

$$[K^{(e)}] = \left([n']^{-1} \right)^T \left[\int [C]^T [D] [C] dA \right] [n']^{-1} \quad \dots \dots \dots (44)$$

where

$$[C] = \begin{bmatrix} 0 & 0 & 0 & 2 & 0 & 0 & 6x & 2y & 0 \\ 0 & 0 & 0 & 0 & 0 & 2 & 0 & 2x & 6y \\ 0 & 0 & 0 & 0 & 2 & 0 & 0 & 4(x+y) & 0 \end{bmatrix} \quad \dots \dots \dots (45)$$

The area integrals appearing inside the bracket of Eq.(44) can be calculated in terms of the global XY coordinate system as well as in terms of local xy system chosen in Figure 16 from the following relations:

$$\iint_{\text{area}} y \, dx dy = \frac{1}{2} x_3 y_2 (y_2 + y_3) \quad \dots \dots \dots (48)$$

$$\iint_{\text{area}} x^2 \, dx \, dy = \frac{1}{12} x_3^3 y_2 \quad \dots \dots \dots (49)$$

$$\iint_{\text{area}} x y \, dx dy = \frac{1}{24} x_3^2 y_2 (y_2 + 2y_3) \quad \dots \dots \dots (50)$$

$$\iint_{x+y=2} y^2 \, dx dy = \frac{1}{12} x_3 y_2 (y_2^2 + y_2 y_3 + y_3^2) \quad \dots \dots \dots (51)$$

Appendix shows the detailed calculations of the local element stiffness

matrix. Finally the element stiffness matrix from Eq.(44) in the global coordinate system whose XY plane is assumed to be same as the local xy plane) can be obtained from

$$[K]^{(e)} = [p]^T \lceil k^{(e)} \rceil [p] \quad \dots \dots \dots (52)$$

where the transformation matrix $[p]$ is given by

$$\begin{bmatrix}
 1 & 0 & 0 & 0 & 0 & 0 & 0 & 0 & 0 \\
 0 & \text{lox} & \text{max} & 0 & 0 & 0 & 0 & 0 & 0 \\
 0 & \text{loy} & \text{moy} & 0 & 0 & 0 & 0 & 0 & 0 \\
 0 & 0 & 0 & 1 & 0 & 0 & 0 & 0 & 0 \\
 0 & 0 & 0 & 0 & \text{lox} & \text{max} & 0 & 0 & 0 \\
 0 & 0 & 0 & 0 & \text{loy} & \text{moy} & 0 & 0 & 0 \\
 0 & 0 & 0 & 0 & 0 & 0 & 1 & 0 & 0 \\
 0 & 0 & 0 & 0 & 0 & 0 & 0 & \text{lox} & \text{max} \\
 0 & 0 & 0 & 0 & 0 & 0 & 0 & \text{loy} & \text{moy}
 \end{bmatrix}
 \quad [p] = \dots \quad (53)$$

where (l_{ox}, m_{ox}) and (l_{oy}, m_{oy}) represent the direction cosines of the lines ox and oy respectively.

After each element stiffness matrix is calculated, it is assembled into the global stiffness matrix. The resultant matrix equation becomes

where $[F]$ is the force matrix.

In order to compute stresses and strains, post-processing is accomplished. After obtaining displacements, local strains are extracted from the global displacements. To this end, the local coordinate, matrix $[n']$,

direction cosines, and the transformation function for each element are calculated. Then, the local strain vector is

where matrix $[H']$ is the same as matrix $[H]$ except that x is one-third of $(x_1+x_2+x_3)$ and y is one-third of $(y_1+y_2+y_3)$ and $z=h$ and $-h$ in order to compute strains at the top and bottom sides of the plate. In addition, $[d]$ is the nodal displacement vector of an element. The local strain is transformed into the global strain by using the following equation:

where

$$[T] = \begin{bmatrix} l_{ox}^2 & m_{ox}^2 & l_{ox} * m_{ox} \\ m_{ox}^2 & l_{ox}^2 & -l_{ox} * m_{ox} \\ -2l_{ox} * m_{ox} & 2l_{ox} * m_{ox} & l_{ox}^2 - m_{ox}^2 \end{bmatrix}$$

At the end, stresses are computed from the strains using Eq. (6). These are the global stresses.

VI. NUMERICAL RESULTS AND DISCUSSION

A. NUMERICAL RESULTS

In order to calculate the strain and stress for a laminated composite plate with a quarter inch hole at the center and subjected to a pure bending moment, a program named MFEM.M is written in Matlab. With an input for material properties, plate dimensions, the applied bending moment, and the failure load of the material, this program calculates the deflection, strain, and failure stress for each element. Another program named DMTRX.M is also written in Matlab which is capable to calculate the stiffness matrix $[\bar{Q}]$ for four different kinds of laminae $[0^\circ]$, $[90^\circ]$, $[0^\circ/90^\circ]_{12}$, and $[(+45^\circ/-45^\circ)_s]$.

In this thesis, a laminated plate with a quarter inch hole at the center is modeled with 214 nodes and 371 elements, which generates 642 by 642 stiffness matrix (642 dof) as shown in Figure 17. After calculations, normalized stresses of stress concentration and the normalized failure stresses v.s the distance away from the circular hole edge for $[0^\circ]_{24}$ and $[0^\circ/90^\circ]_{12}$ are plotted in Figure 18 through 23. As a result, the stress concentration factor calculated from the F.E. analyses for the $[0^\circ]_{24}$ laminate is 1.47 and that for the $[0^\circ/90^\circ]_{12}$ is 1.27. Normalized failure stresses for the

$[0^\circ]_{24}$ laminate, the top $[0^\circ]$ layer and bottom $[90^\circ]$ layer of the $[0^\circ/90^\circ]_{12}$ laminate are all close to one at the edge of the hole.

B. DISCUSSION

Whitney and Nuismer [Ref. 7] said that when the stress at a characteristic distance, d_0 , away from the discontinuity would be equal to or greater than the strength of the unnotched material, failure would occur. In this current work, the constant value, d_0 , for the $[0^\circ]_{24}$ and $[0^\circ/90^\circ]_{12}$ laminae is zero from the results. Thus, the failure criterion of Whitney and Nuismer assumption is not suitable in this kind of graphite fiber/epoxy. Since it is of great importance for design purpose to be able to predict the strength of a composite under loading conditions prevailing in service, some failure criteria like the maximum stress criterion and the Tsai-Hill failure criterion are used in order to predict the failure and check the failure criteria.

1. Maximum Stress Criterion

This criterion tells that failure will occur when any one of stress components is equal to or greater than its corresponding allowable strength. Since the stress in the x-direction is the dominant stress in this current work, failure will occur when

$$\sigma_1 \geq x_1^T \quad \dots \dots \dots (57)$$

where X_{11}^T is the ultimate uniaxial tensile strength in the fiber direction (in this case, x-direction).

2. Tsai-Hill Criterion

According to the Tsai-Hill criterion, failure of an orthotropic lamina will occur under a general stress state when

$$\frac{\sigma_1^2}{x^2} - \frac{\sigma_1 \sigma_2}{xy} + \frac{\sigma_2^2}{y^2} + \frac{\sigma_{12}^2}{S^2} \geq 1 \quad \dots \dots \dots (58)$$

where X , Y , and S are the longitudinal tensile failure strength, the transverse tensile failure strength, and the in-plane shear failure strength, respectively.

Figures 7 through 14 show that for this particular laminated composite failure occurred almost simultaneously on both compressive and tensile sides. From figures of normalized failure stresses, it is obvious that failure occurred at the hole edge when the stresses at the hole edge were equal to their corresponding allowable strengths.

Stress concentration factors obtained from the experiments and numerical analyses are nearly the same for both $[0^\circ]_{24}$ and $[0^\circ/90^\circ]_{12}$.

laminated plates. This result confirm that failure occurs when the maximum stress at the edge of a hole is the same as the material strength.

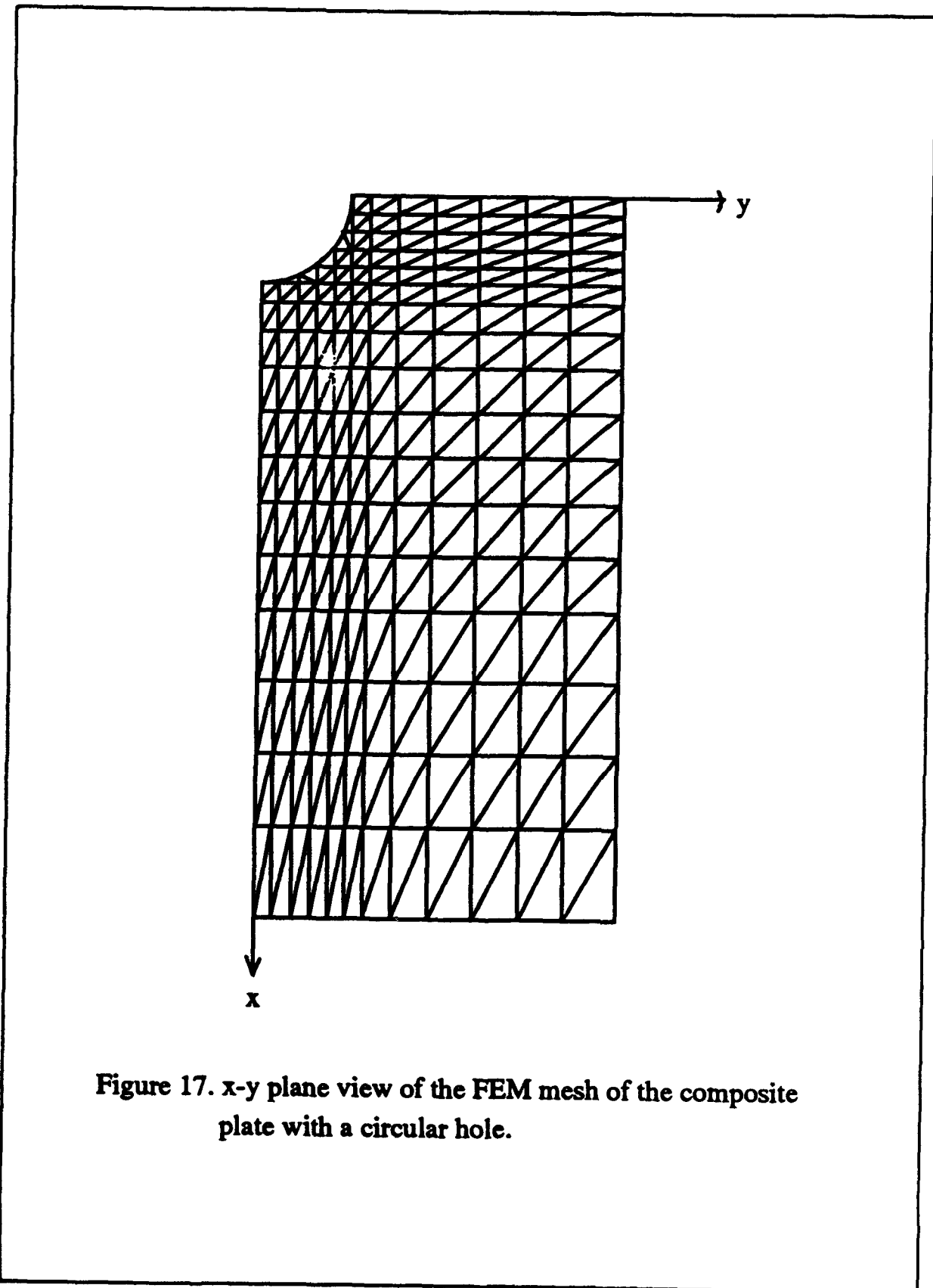


Figure 17. x-y plane view of the FEM mesh of the composite plate with a circular hole.

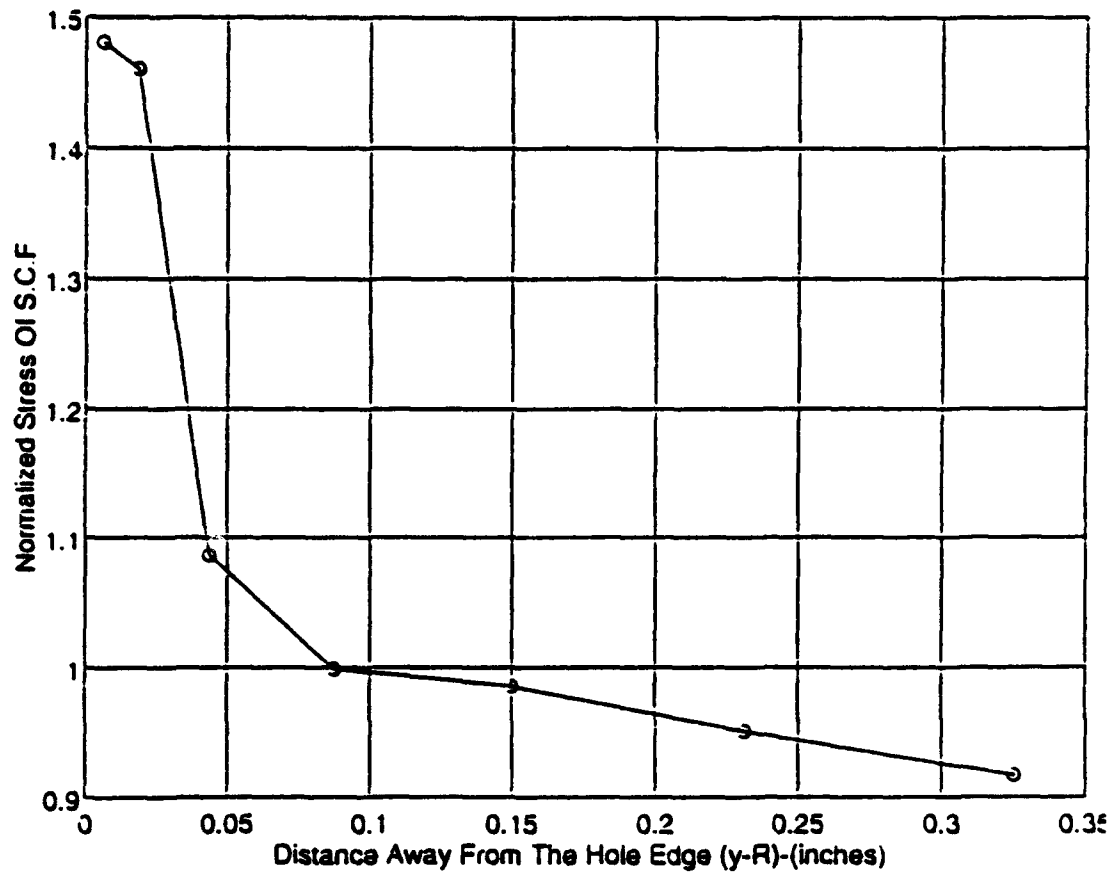


Figure 18. Stress concentration factor for [0] laminate

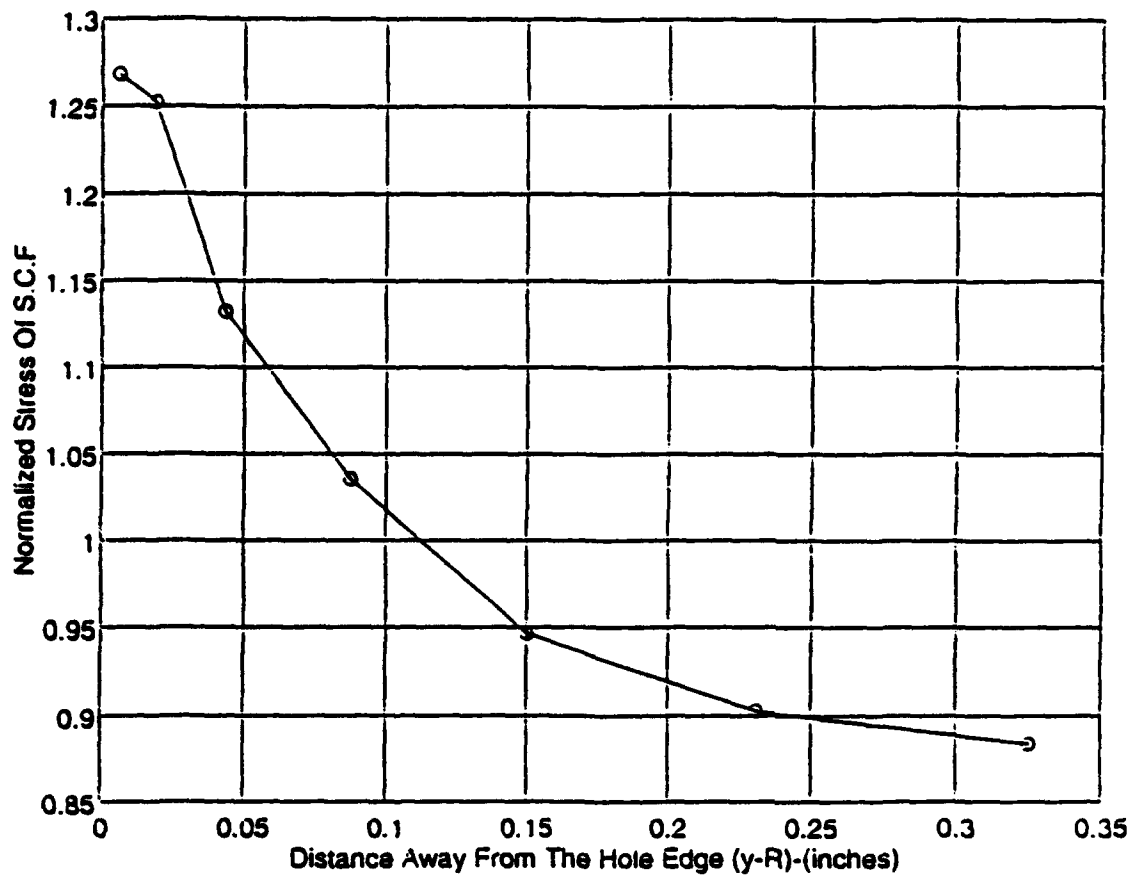


Figure 19. Stress concentration factor for [0/90] laminate at top layer-[0]

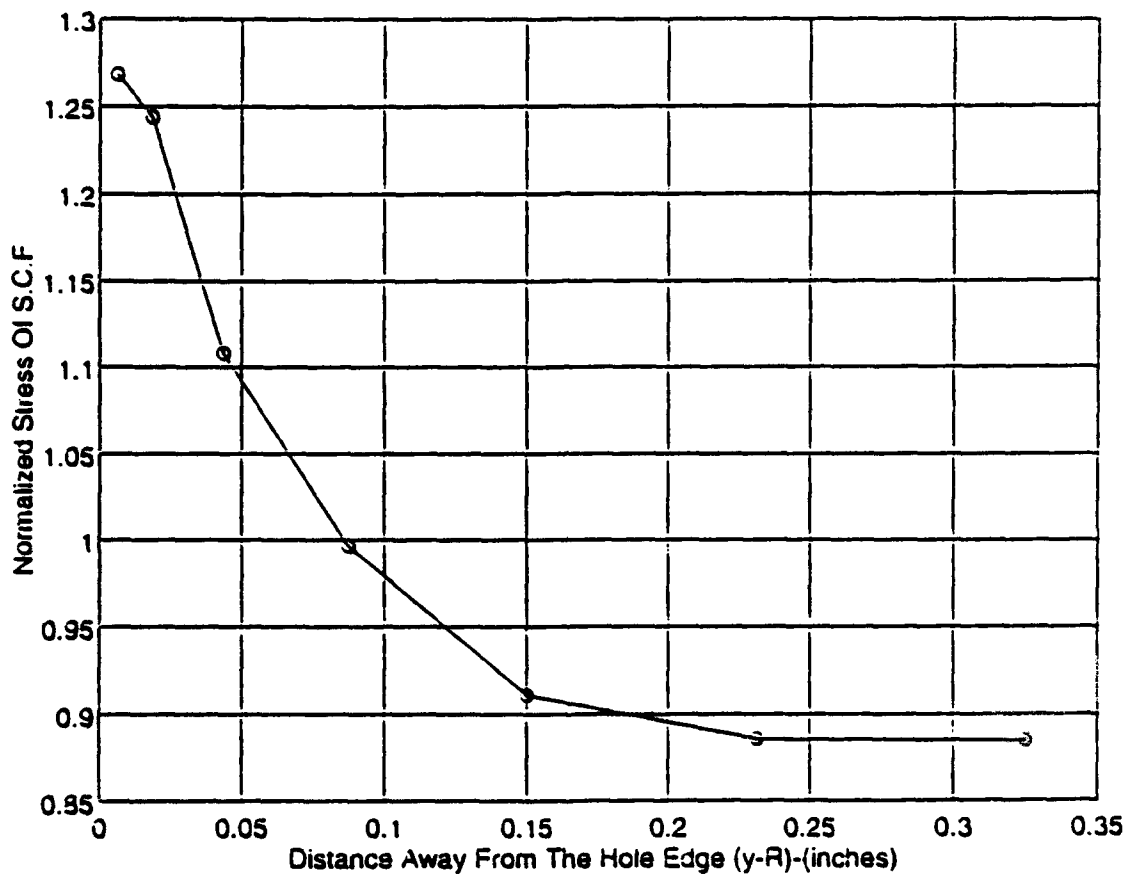


Figure 20. Stress concentration factor for [0/90] laminate at bottom layer-[90]

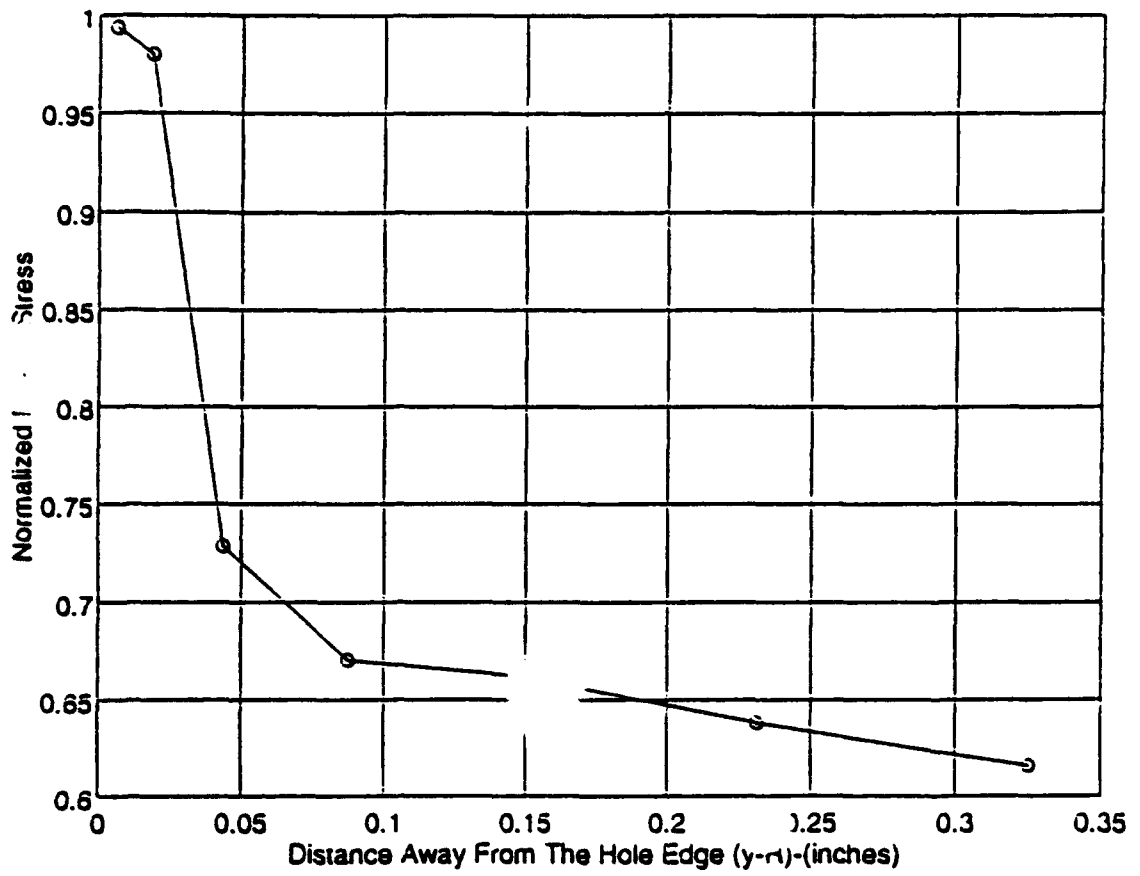


Figure 21. Stress distributions for [0] laminate

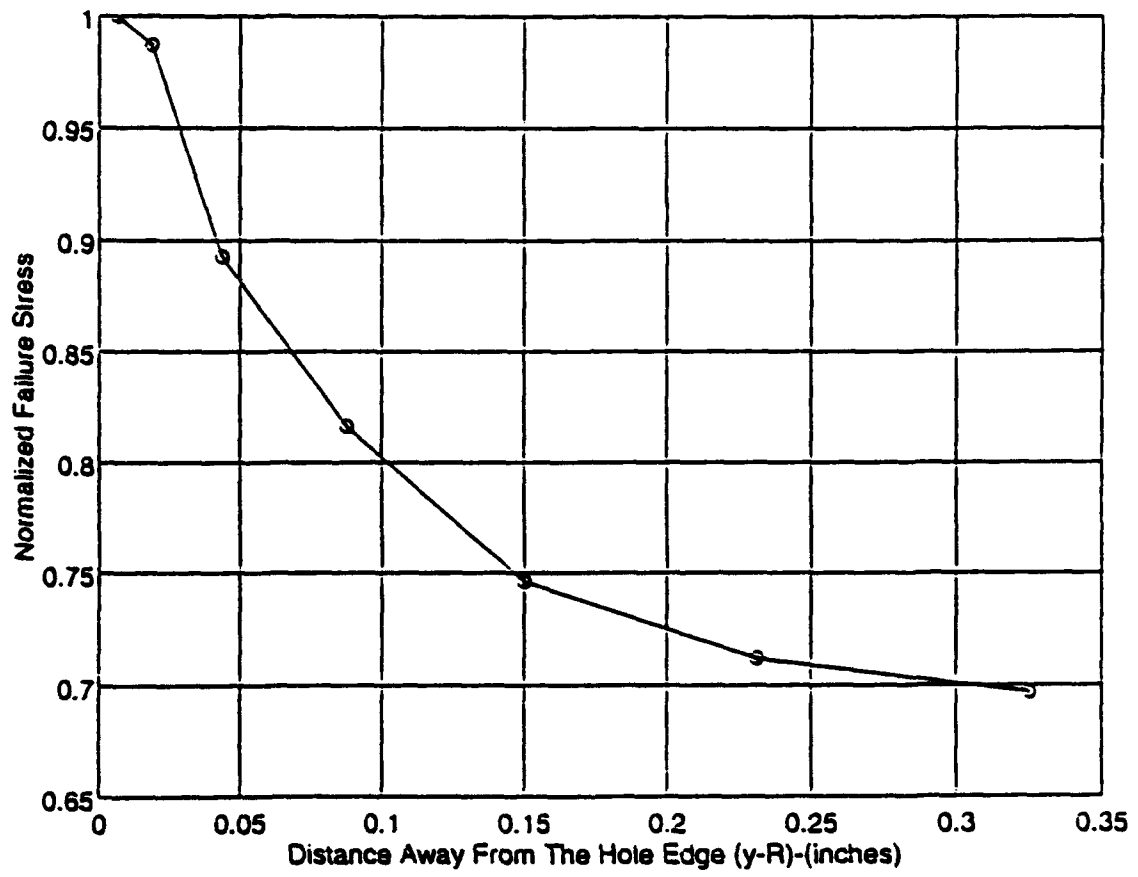


Figure 22. Stress distributions for [0/90] laminate at top layer-[0]

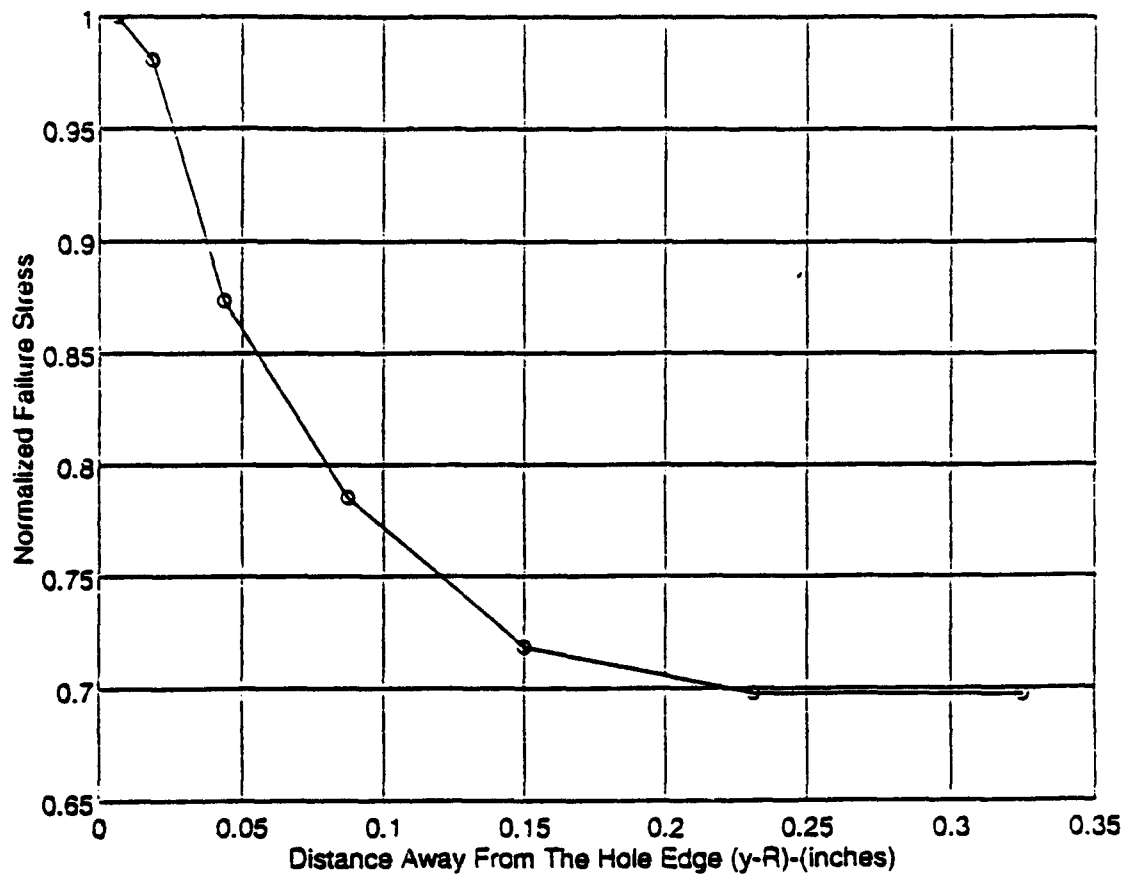


Figure 23. Stress distributions for [0/90] laminate at bottom layer-[90]

VII. CONCLUSIONS

In this thesis, a four-point bending test is used to investigate the failure strain and failure stress for a graphite-fiber/epoxy composite of four different laminated plates. From experimental results, composite elastic modulii are obtained and the stress concentration factors due to a quarter inch hole located at the center of the plate are calculated. Furthermore, a numerical analysis using the finite element method is conducted to simulate the plate under the same loading condition. By using both experimental and numerical results, the characteristic distance d_0 , which determines failure based on the Whitney and Nuismer theory, is examined. Finally, the maximum stress criterion and the Tsai-Hill failure criterion is applied to check the failure of composite. These failure criteria confirm that failure occurs when the dominant stress component of the laminated composite is equal to its maximum allowable strength. From this work, it is also concluded that:

- the four-point bending test is a good way to investigate material properties although it is a little more complicated to conduct than the tensile test.

- The characteristic distance for the Whitney and Nuismer theory is zero for the present composite material. Both the maximum stress criterion and Tsai-Hill failure criterion are proper to predict the failure for this material.

APPENDIX

The $[n']$ matrix in Equation (37) is

$$[n'] = \begin{bmatrix} 1 & 0 & 0 & 0 & 0 & 0 & 0 & 0 & 0 \\ 0 & 0 & 1 & 0 & 0 & 0 & 0 & 0 & 0 \\ 0 & -1 & 0 & 0 & 0 & 0 & 0 & 0 & 0 \\ 1 & 0 & y_2 & 0 & 0 & y_2^2 & 0 & 0 & y_2^3 \\ 0 & 0 & 1 & 0 & 0 & 2y_2 & 0 & 0 & 3y_2^2 \\ 0 & -1 & 0 & 0 & -y_2 & 0 & 0 & -y_2^2 & 0 \\ 1 & x_3 & y_3 & x_3^2 & x_3y_3 & y_3^2 & x_3^3 & (x_3^2y_3 + x_3y_3^2) & y_3^3 \\ 0 & 0 & 1 & 0 & x_3 & 2y_3 & 0 & (2x_3y_3 + x_3^2) & 3y_3^2 \\ 0 & -1 & 0 & -2x_3 & -y_3 & 0 & -3x_3^2 & -(y_3^2 + 2x_3y_3) & 0 \end{bmatrix}$$

The detail calculations of $[C]^T[D][C]$ in Equation (44) are shown as

$$[C]^T[D] = \begin{bmatrix} 0 & 0 & 0 \\ 0 & 0 & 0 \\ 0 & 0 & 0 \\ 2 & 0 & 0 \\ 0 & 0 & 2 \\ 0 & 2 & 0 \\ 6x & 0 & 0 \\ 2y & 2x & 4(x+y) \\ 0 & 6y & 0 \end{bmatrix}_{9 \times 3} \begin{bmatrix} D_{11} & D_{12} & D_{16} \\ D_{12} & D_{22} & D_{26} \\ D_{16} & D_{26} & D_{66} \end{bmatrix}_{3 \times 3}$$

$$[C]^T[D] = \begin{bmatrix} 0 & 0 & 0 \\ 0 & 0 & 0 \\ 0 & 0 & 0 \\ 2D_{11} & 2D_{12} & 2D_{16} \\ 2D_{16} & 2D_{26} & 2D_{66} \\ 2D_{12} & 2D_{22} & 2D_{26} \\ 6xD_{11} & 6xD_{12} & 6xD_{16} \\ \Delta_1 & \Delta_2 & \Delta_3 \\ 6yD_{12} & 6yD_{22} & 6yD_{26} \end{bmatrix}$$

where

$$\begin{aligned} \Delta_1 &= 2yD_{11} + 2xD_{12} + 4(x+y)D_{16} \\ \Delta_2 &= 2yD_{12} + 2xD_{22} + 4(x+y)D_{26} \\ \Delta_3 &= 2yD_{16} + 2xD_{26} + 4(x+y)D_{66} \end{aligned}$$

and

$$[C]^T[D][C] = \begin{bmatrix} 0 & 0 & 0 & 0 & 0 & 0 & 0 & 0 \\ 0 & 0 & 0 & 0 & 0 & 0 & 0 & 0 \\ 0 & 0 & 0 & 0 & 0 & 0 & 0 & 0 \\ 0 & 0 & 0 & 4D_{11} & 4D_{16} & 4D_{12} & 12xD_{11} & \Delta_4 & 12yD_{12} \\ 0 & 0 & 0 & 4D_{16} & 4D_{66} & 4D_{26} & 12xD_{16} & \Delta_5 & 12yD_{26} \\ 0 & 0 & 0 & 4D_{12} & 4D_{26} & 4D_{22} & 12xD_{12} & \Delta_6 & 12yD_{22} \\ 0 & 0 & 0 & 12xD_{11} & 12xD_{16} & 12xD_{12} & 36x^2D_{11} & \Delta_7 & 36xyD_{12} \\ 0 & 0 & 0 & \Delta_4 & \Delta_5 & \Delta_6 & \Delta_7 & \Delta_8 & \Delta_9 \\ 0 & 0 & 0 & 12yD_{12} & 12yD_{26} & 12yD_{22} & 36xyD_{12} & \Delta_9 & 36y^2D_{22} \end{bmatrix}$$

$$\Delta_4 = (4D_{12} + 8D_{16})x + (4D_{11} + 8D_{16})y$$

$$\Delta_5 = (4D_{26} + 8D_{66})x + (4D_{16} + 8D_{66})y$$

$$\Delta_6 = (4D_{22} + 8D_{26})x + (4D_{12} + 8D_{26})y$$

$$\Delta_7 = (12D_{12} + 24D_{16})x^2 + (12D_{11} + 24D_{16})xy$$

$$\begin{aligned}\Delta_8 = & (4D_{22} + 16D_{26} + 16D_{66})x^2 + (8D_{12} + 16D_{16})xy \\ & + (16D_{26} + 32D_{66})xy + (4D_{11} + 16D_{16} + 16D_{66})xy\end{aligned}$$

$$\Delta_9 = (12D_{22} + 24D_{26})xy + (12D_{12} + 24D_{26})y^2$$

Thus, the area integrals inside the bracket of Eq.(44) can be obtained

$$\iint_A [C]^T [D] [C] dA = \begin{bmatrix} 0 & 0 & 0 & 0 & 0 & 0 & 0 \\ 0 & 0 & 0 & 0 & 0 & 0 & 0 \\ 0 & 0 & 0 & 0 & 0 & 0 & 0 \\ 0 & 0 & 0 & A_1 & A_2 & A_4 & A_7 \\ 0 & 0 & 0 & A_2 & A_3 & A_5 & A_8 \\ 0 & 0 & 0 & A_4 & A_5 & A_6 & A_9 \\ 0 & 0 & 0 & A_7 & A_8 & A_9 & A_{10} \\ 0 & 0 & 0 & A_{11} & A_{12} & A_{13} & A_{14} \\ 0 & 0 & 0 & A_{16} & A_{17} & A_{18} & A_{19} \end{bmatrix}$$

where : $A_1 = 2D_{11}x_3y_2, \quad A_2 = 2D_{16}x_3y_2,$
 $A_3 = 2D_{66}x_3y_2, \quad A_4 = 2D_{12}x_3y_2,$
 $A_5 = 2D_{26}x_3y_2, \quad A_6 = 2D_{22}x_3y_2,$
 $A_7 = 2D_{11}x^2_3y_2, \quad A_8 = 2D_{16}x^2_3y_2,$
 $A_9 = 2D_{12}x^2_3y_2, \quad A_{10} = 3D_{11}x^3_3y_2,$
 $A_{11} = (4D_{12} + 8D_{16})(x^2_3y_2)/6 + (4D_{11} + 8D_{16})[x_3y_2(y_2 + y_3)/6],$
 $A_{12} = (4D_{26} + 8D_{66})(x^2_3y_2)/6 + (4D_{16} + 8D_{66})[x_3y_2(y_2 + y_3)/6],$
 $A_{13} = (4D_{22} + 8D_{26})(x^2_3y_2)/6 + (4D_{12} + 8D_{26})[x_3y_2(y_2 + y_3)/6],$
 $A_{14} = (12D_{12} + 24D_{16})(x^3_3y_2)/12 + (12D_{11} + 24D_{16})[x^2_3y_2(y_2 + 2y_3)/24],$
 $A_{15} = (4D_{22} + 16D_{26} + 16D_{66})(x^3_3y_2)/12$
 $+ (8D_{12} + 16D_{16} + 16D_{26} + 32D_{66})[x^2_3y_2(y_2 + 2y_3)/24]$
 $+ (4D_{11} + 16D_{16} + 16D_{66})[x_3y_2(y^2_2 + y_2y_3 + y^2_3)/12],$
 $A_{16} = 2D_{12}x_3y_2(y_2 + y_3), \quad A_{17} = 2D_{26}x_3y_2(y_2 + y_3),$
 $A_{18} = 2D_{22}x_3y_2(y_2 + y_3), \quad A_{19} = 3D_{12}x^2_3y_2(y_2 + 2y_3),$
 $A_{20} = (12D_{22} + 24D_{26})[x^2_3y_2(y_2 + 2y_3)/24]$
 $+ (12D_{12} + 24D_{26})[x_3y_2(y^2_2 + y_2y_3 + y^2_3)/12],$
 $A_{21} = 3D_{22}x_3y_2(y^2_2 + y_2y_3 + y^2_3).$

LIST OF REFERENCES

- [1] J. D. Sipes, Real Admiral, USCG Chairman, "SSC-360 Use of Fiber Reinforced Plastics in the Marine Industry", Ship Structure Committee, September 1990.
- [2] A. G. H. Dietz, *Engineering Laminates*, Wiley (1949).
- [3] N. J. Pagano, "Analysis of The Flexure Test of Bidirectional Composites", *J. Composite Materials*, Vol. 1 (1967), p. 336.
- [4] H. T. Hahn and S. W. Tsai, "Graphical Determination of Stiffness and Strength of Composite Laminates", *J. Composite Materials*, Vol. 8 (April 1974), p. 160.
- [5] Kirsch, G., *VDI*, VOL. 42, 1898.
- [6] J. M. Whitney and R. J. Nuismer, "Stress Fracture Criteria for Laminated Composites Containing Stress Concentrations", *J. Composite Materials*, Vol. 8 (July 1974), p. 253.
- [7] H. J. Konish and J. M. Whitney, "Approximate Stresses in an Orthotropic Plate Containing a Circular Hole", *J. Composite Materials*, Vol.9 (April 1975), p.157.
- [8] N. J. Hoff and C. Muser, "Stress Concentration Factors for Cylindrically Orthotropic Plates", *J. Composite Materials*, Vol.16 (July 1982), p. 313.
- [9] Fu-Kuo Chang and Kuo-Yen Chang, "A Progressive Damage Model for Laminated Composites Containing Stress Concentrations", *J. Composite Materials*, Vol. 21 (September 1987), p. 834.

- [10] J. L. Batoz, K. J. Bathe, and L. W. Ho, "A Study of Three-Node Triangular Plate Bending Element", International Journal for Numerical Method in Engineering, 15, 1771-1812, 1980.
- [11] J. L. Batoz, "An Explicit Formulation for an Efficient Triangular Plate Bending Element", International Journal for Numerical Method in Engineering, 18, 1077-1089, 1982.
- [12] A. J. Fricker, "An Improved Three-Noded Triangular Element for Plate Bending", International Journal for Numerical Method in Engineering, 21, 105-114, 1985.
- [13] S. W. Lee and J. C. Zhang, "A Six-Node Finite Element for Plate Bending", International Journal for Numerical Method in Engineering, 21, 131-143, 1985.
- [14] J. L. Tocher, "Analysis of Plate Bending Using Triangular Elements", Ph.D Dissertation, University of California, Berkeley, 1962.

INITIAL DISTRIBUTION LIST

- | | |
|---|----------|
| 1. Defense Technical Information Center
Cameron Station
Alexandria, VA 22304-6145 | 2 |
| 2. Library, Code 52
Naval Postgraduate School
Monterey, CA 93943-5101 | 2 |
| 3. Professor Y. W. Kwon, Code ME/Kw
Department of Mechanical Engineering
Naval Postgraduate School
Monterey, CA 93943-5000 | 2 |
| 4. Department Chair, Code ME/Kk
Department of Mechanical Engineering
Naval Postgraduate School
Monterey, CA 93943-5000 | 1 |
| 5. Dr. Shaio-Wen Wang
Advanced Metallic & Ceramic Branch (6063)
Aircraft Division
Naval Air Warfare Center
Warminster, PA 18974-0591 | 1 |
| 6. Dr. Roland Cochran
Ploymer Composite Branch
Aircraft Division
Naval Air Warfare Center
Warminster, PA 18974-0591 | 1 |

- | | |
|--|----------|
| 7. Mr. David Bonnani
Naval Surface Warfare Center, Carderock Div.
Code 1720.2
Bethesda, MD 20084-5000 | 1 |
| 8. Mr. Erik A. Rasmussen
Naval Surface Warfare Center, Carderock Div.
Code 1720.4
Bethesda, MD 20084-5000 | 1 |
| 9. Dr. Phillip B. Abraham
Office of Naval Research Mechanics Div.
code 332
800 North Quincy Street
Arlington, VA 22217-5000 | 1 |
| 10. Maj. Shih-Ting Yang
4F No. 9 Alley 3 Lane 80 Kai-Hsien 4th Rd.
Kaohsiung, Taiwan
R.O.C. | 4 |